Robust Low-Cost Water-Gas Shift Membrane Reactor For High-Purity Hydrogen Production from Coal-Derived Syngas

Final Technical Report

For Period

June 1, 2005 – May 31, 2008

James Torkelson, Neng Ye, Zhijiang Li, Decio Coutinho and Mark Fokema
Aspen Products Group
186 Cedar Hill Street
Marlborough, MA 01752

August 2008

DOE Award #
DE-FC26-05NT42452

ASPEN PRODUCTS GROUP, INC.

DISCLAIMER

ABSTRACT

This report details work performed in an effort to develop a low-cost, robust water gas shift membrane reactor to convert coal-derived syngas into high purity hydrogen. A sulfur- and halide-tolerant water gas shift catalyst and a sulfur-tolerant dense metallic hydrogen-permeable membrane were developed. The materials were integrated into a water gas shift membrane reactor in order to demonstrate the production of >99.97% pure hydrogen from a simulated coal-derived syngas stream containing 2000 ppm hydrogen sulfide.

TABLE OF CONTENTS

LIST OF TABLES

LIST OF FIGURES

1. EXECUTIVE SUMMARY

This report summarizes the results of the research and development program conducted by Aspen Products Group, Inc. in an effort to develop a low-cost, robust water gas shift membrane reactor to convert coal-derived syngas into high purity hydrogen. The development activities took place between June 1, 2005 and May 31, 2008.

The objectives of the program were to 1) develop a contaminant-tolerant water gas shift catalyst that is able to achieve equilibrium carbon monoxide conversion at high space velocity and low steam to carbon monoxide ratio, 2) develop a contaminant-tolerant hydrogen-permeable membrane with a higher permeability than palladium, 3) demonstrate 1 L/h purified hydrogen production from coal-derived syngas in an integrated catalytic membrane reactor, and 4) conduct a cost analysis of the developed technology.

Sixteen different water gas shift catalysts were prepared or procured and characterized by X-ray diffraction, electron microscopy, and gas adsorption. Catalytic screening tests were conducted to assess which catalyst exhibited the highest water gas shift activity in the presence of H_2S and HCl. Equilibrium carbon monoxide conversions were achieved with high steam content syngas streams ($H_2O/CO=4$, 500°C, 400 psig, 12,000 h^{-1} space velocity) and with drier syngas streams ($H_2O/CO=0.8$, 425°C, 225 psig, 1,400 h^{-1} space velocity) over a custom-synthesized molybdenum-based catalyst. The most active and stable catalyst was operated for over 110 hours in the presence of 3000 ppm H_2S and 350 ppm HCl without irreversible degradation of catalytic activity.

Seventy-five different hydrogen permeable membrane catalysts were prepared, with many characterized by X-ray diffraction, electron microscopy, energy dispersive X-ray analysis, and Auger emission spectroscopy. The effects of membrane substrate cleaning procedure, substrate thickness, coating conditions, coating composition, coating thickness, and annealing conditions on membrane structure were assessed. The effects of exposure to H_2, CO, CO_2, H_2O, and H_2S on membrane permeability and stability at temperatures between 300 and 550°C and transmembrane pressures of up to 400 psi were evaluated. The best performing membrane exhibited a hydrogen permeability of $9x10^{-8}$ mol/m/s/$Pa^{0.5}$ in pure hydrogen at 425°C, six times greater than that of palladium at the same temperature. In the presence of 2000 ppm H_2S a hydrogen permeability of $7x10^{-8}$ mol/m/s/$Pa^{0.5}$ was demonstrated. Membrane embrittlement was a problem at low temperature and high pressure, but was minimized by careful selection and control of membrane operating conditions. Mild embrittlement necessitated the use of moderately thick membranes that restricted the hydrogen flux through the membrane.

The contaminant-tolerant water gas shift catalyst and hydrogen permeable membrane were integrated into a tubular catalytic membrane reactor and evaluated with a simulated coal-derived syngas stream. Production of over 3 L/h hydrogen with purity in excess of 99.97% was demonstrated from syngas containing H_2, CO, CO_2 and H_2O. Exposure of the membrane to CO concentrations in excess of 5% CO resulted in deterioration of membrane performance.

An analysis of the cost of producing the hydrogen permeable membrane indicated that the DOE 2015 hydrogen permeable membrane cost target could be achieved. All 2015 development targets could be achieved by the membrane except H_2 flux and transmembrane pressure capability. In order to achieve these targets, thinner membranes with enhanced mechanical strength are required.

2. INTRODUCTION

Coal gasification is one of the most efficient ways to convert coal into electricity, hydrogen and other valuable products. In a typical gasifier, coal is reacted with steam and air at high temperature and high pressure to produce syngas, which is a mixture of hydrogen, carbon monoxide and other gaseous products. Unwanted impurities, such as hydrogen sulfide, heavy metals, and even carbon dioxide, can be absorbed from the syngas yielding a product stream well-suited for power generation and chemical synthesis.

Use of the syngas in a combined cycles plant may yield electrical power generation efficiencies of greater than 45%, compared to approximately than 35% in conventional coal generation plants. Incorporation of fuel cells into the plant offers great potential for further efficiency improvements. Reductions in the cost of hydrogen production from coal are required to capitalize on this opportunity.

The conventional route of hydrogen production from syngas makes use of water gas sift units, contaminant scrubbers and pressure swing adsorbers. Coupling of hydrogen premeable membranes with water gas shift catalysts offers the potential for pure hydrogen production in a single unit operation.

The Department of Energy, in its 2007 Hydrogen from Coal Program RD&D Plan,[1] established technical objectives for water gas shift catalysts and hydrogen permeable membranes, as summarized in Table I and Table II. Critical shortcomings of current water gas shift catalysts include cost, operation at low steam/CO ratios, and impurity tolerance. The primary shortcomings of current membranes include cost, durability and H_2 flux.

Table I: DOE Water Gas Shift Development Targets[1]

Performance Criteria	Units	Current Status	2010	2015
Reactor Type	-	Multiple fixed beds	Advanced configurations - tbd	
Catalyst Form	-	Pellets	Advanced configurations - tbd	
Active Metal	-	Cu/Zn or Fe/Cr or Co/Mo	Advanced configurations – tbd	
Feed Temperature	°C	200–300	>250	>400
Feed Pressure	psia	450–1150	>450	>750
Approach to Equilibrium	°C	8–10	<6	<4
Min. Steam/CO Ratio	Molar	2.6	<2.6	<2
Sulfur Tolerance, ppmv	-	Varies	>20	>100
COS Conversion	-	Varies	Partial	Total
Chloride Tolerance, ppmv	-	Varies	> 3	>100
Stability/Durability	Years	3–7	>7	>10
Catalyst Cost	$/lb	~5	<5	<5

Table II: DOE Hydrogen Permeable Membrane Development Targets[1]

Performance Criteria	Units	Current Status [a] (H_2-permeable cermet)	2007 Target	2010 Target	2015 Target
Flux [b]	$ft^3/hour/ft^2$	~220	100	200	300
Temperature	°C	300–400	400–700	300–600	250–500
S Tolerance	ppmv	Yes (~20 ppmv)	----	20	>100
Cost	$\$/ft^2$	<200	150	100	<100
WGS Activity	-	N/A	Yes	Yes	Yes
ΔP Operating Capability [c]	psi	1,000 (tested)	100	Up to 400	Up to 800 to 1,000
Carbon Monoxide Tolerance	-	Yes	Yes	Yes	Yes
Hydrogen Purity [d]	%	>99.999%	95%	99.5%	99.99%
Stability/Durability	years	0.9 (tested)	1	3	5

The primary advantage of coupling the water gas shift reaction with H_2 permeable membranes in a single operation is the ability to circumvent the thermodynamic equilibrium limitations associated with conventional catalytic reactors. The water gas shift reaction,

$$CO + H_2O \leftrightarrow CO_2 + H_2 \qquad \Delta H_R = -41.2 \text{ kJ/mol} \qquad (1)$$

is a reversible reaction in which build up of reaction products, CO_2 and H_2, limits the level of CO conversion and H_2 yield that can be accomplished at a particular temperature. Figure 1 shows the maximum H_2 yield that can be obtained as a function of temperature and H_2O/CO ratio for a hypothetical coal-derived syngas feed containing 25% H_2, 59.7% CO, 10% CO_2, 5% N_2, and 3000 ppm H_2S. At the more desirable low H_2O/CO ratios, only 90% H_2 yield can be achieved at 450°C and 400 psig.

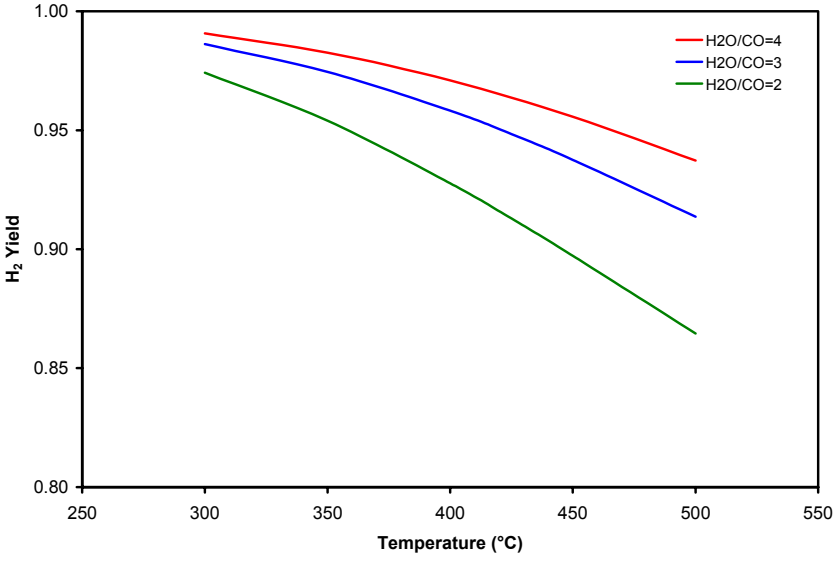

Figure 1: Equilibrium H_2 Yield without Active Removal of H_2 Product
(25% H_2, 59.7% CO, 10% CO_2, 5% N_2, 3000 ppm H_2S; Press.=400 psig)

Active removal of H_2 from the reaction zone enables the water gas shift reaction to proceed to the right at CO conversions approaching 100%. Figure 2 presents a plot of hydrogen yields that can be achieved in a membrane reactor operating at $H_2O/CO=2$ in which H_2 is removed as it is produced so that the partial pressure of H_2 in the reactor is maintained at 1 atm. The total amount of H_2 produced in the membrane reactor is 99% of the theoretical maximum at 450°C and 400 psig. Of that amount, 93% is recovered as purified hydrogen, while 7% remains in the syngas mixture. At higher pressures, the benefits of the membrane reactor approach become even more significant.

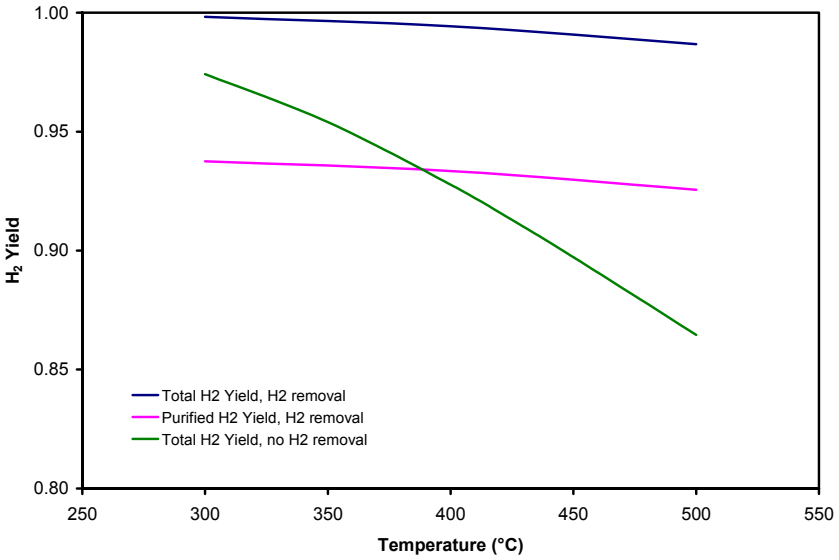

Figure 2: Equilibrium H_2 Yield with Active Removal of H_2 Product
(25% H_2, 59.7% CO, 10% CO_2, 5% N_2, 3000 ppm H_2S; $H_2O/CO=2$; Press.=400 psig)

Methanation of CO is a concern in syngas processing systems.

$$CO + 3H_2 \leftrightarrow CH_4 + H_2O \qquad \Delta H_R = -206 \text{ kJ/mol} \qquad (2)$$

The production of methane significantly reduces H_2 yield, so the methanation activity of water gas shift catalysts must be minimized. Figure 3 presents the equilibrium H_2 yield for non-membrane water gas shift systems in which methanation does and does not take place. Methanation reduces the H_2 yield from 90 to 7%. Thus, it is vitally important to develop catalysts that are active only for WGS shift reaction.

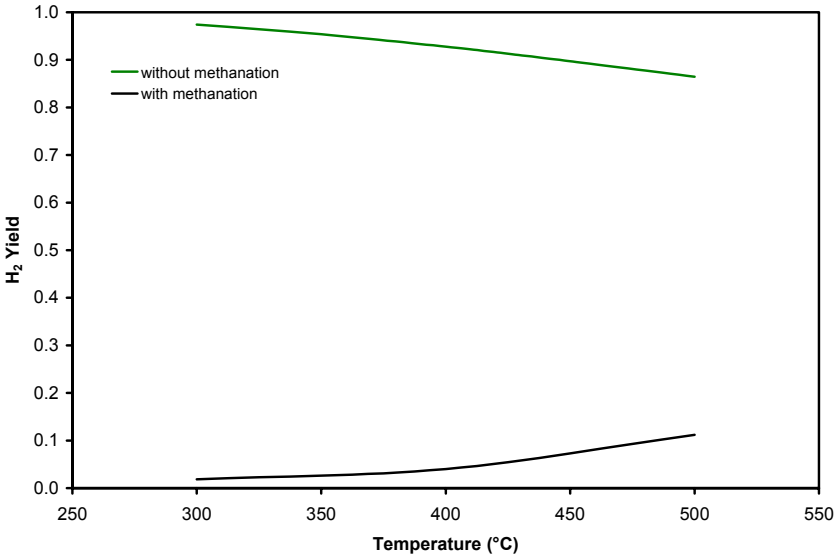

Figure 3: Effect of Methanation Reaction on H_2 Yield
(25% H_2, 59.7% CO, 10% CO_2, 5% N_2, 3000 ppm H_2S; H_2O/CO=2; Press.=400 psig)

3. WATER GAS SHIFT CATALYST DEVELOPMENT

3.1. CATALYST PREPARATION

Sixteen WGS catalysts were prepared or purchased during the course of this program. These included several series of fourteen transition metal-based catalysts prepared in-house and two commercial catalysts, C1 and C2. C1 was a conventional Fe_3O_4/Cr_2O_3 high temperature shift catalyst, while C2 was a Co/MoS_2 sour gas shift catalyst.

Bulk, unsupported MCC and MCH series catalysts were synthesized by evaporation of metal salt solutions at 100°C and calcination in air at 500 ºC for 3h to form metal oxide, followed by heat treatment between 550 and 650ºC in a reducing atmosphere.

For Al_2O_3-supported MCH catalysts, commercial alumina beads in the size of 1/16" in diameter, were used as the support. MCH/Al_2O_3 was prepared by impregnation of the alumina beads with metal salt solutions, followed by heat treatment at 615ºC for 3 hours in a reducing atmosphere.

Supported MCP catalysts containing molybdenum and other transition metal oxides were prepared in a similar fashion to the Al_2O_3-supported MCH catalysts.

Other catalysts were first prepared by successive stepwise impregnation of an alumina support with aqueous metal nitrate solutions. After each impregnation step, drying at 80 ºC overnight was performed. The products were finally calcined at 550ºC for 5 h to produce the catalysts in the desired oxide forms.

3.2. CATALYST CHARACTERIZATION

The WGS catalysts were characterized to determine their surface area, pore size, agglomerate size and composition. BET surface area and pore volume were measured using a Micromeritics ASAP 2010 gas adsorption analyzer. Crystalline phases were determined via powder X-ray diffraction (XRD) analysis using a Rigaku D/MAX-B X-ray diffractometer with a Cu anode. Catalyst microstructure was analyzed by scanning electron microscopy (SEM).

Results of gas adsorption analyses are presented in Table III. Surface areas of supported catalysts were typically in the range of 130-200 m^2/g, much higher than those of unsupported materials. The supported catalyst pore volumes were also higher, at ~0.4 cm^3/g. Analysis of the MCP series of catalysts (alumina-supported multicomponent transition metal oxides) revealed that with the increase of total transition metal oxide loading, both the surface area and pore volume decreased. However, among all the catalysts prepared, the MCP catalysts had the highest surface area and pore volume. The pore size distribution of catalyst MCP-3 is presented in Figure 4.

XRD analysis of the alumina-supported catalysts (Figure 5) revealed amorphous active phases supported on crystalline alumina. Well developed crystalline phases were identified in the unsupported MCC catalysts.

Table III: Physical Properties of Water Gas Shift Catalysts

Catalyst	Surface Area (m^2/g)	Pore Volume (cm^3/g)
MCC-550	-	-
MCC-600	3.1	0.01
MCC-650	14.3	0.02
MCH-15	-	-
MCH-30	25.5	0.01
MCH-50	-	-
MCH/Al_2O_3	155	0.43
MO/Al_2O_3	146	0.40
MCP/Al_2O_3	138	0.39
CC/Al_2O_3	153	0.37
MCP-1	200	0.50
MCP-2	177	0.44
MCP-3	147	0.36
MCP-4	77.3	0.21
C1	199	0.51
C2	83.7	0.31

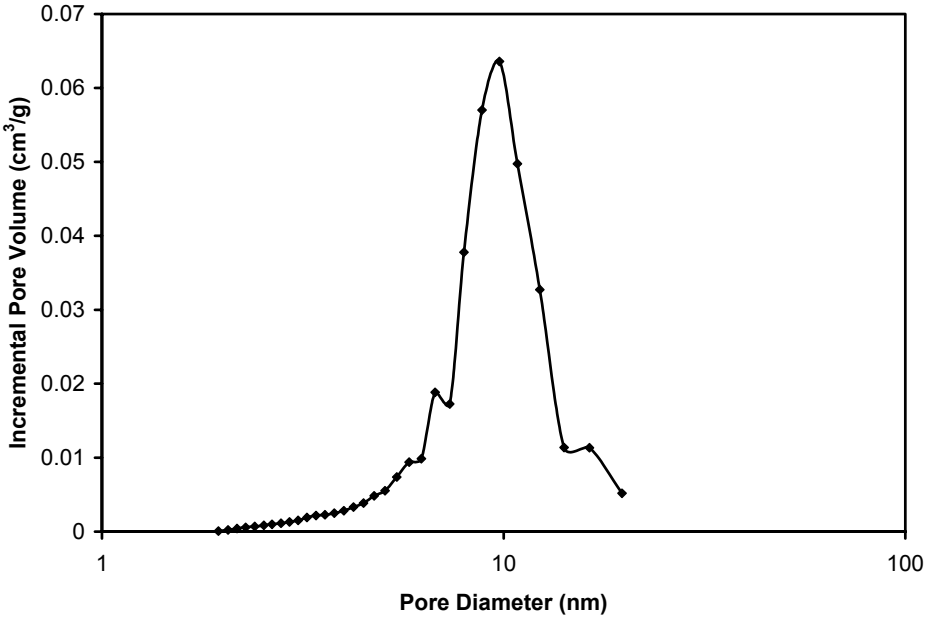

Figure 4: Pore Size Distribution of MCP-3

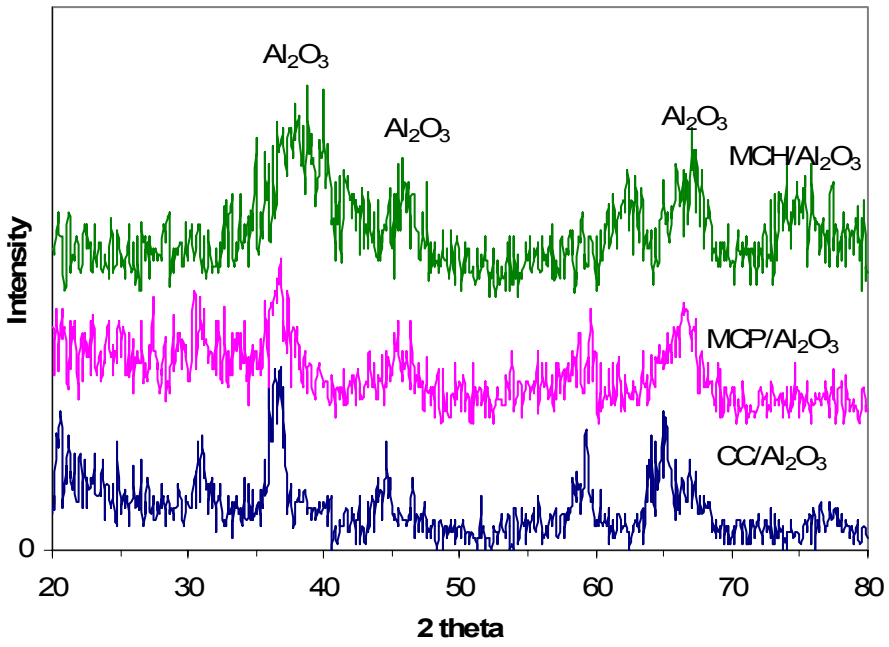

Figure 5: XRD Patterns of Al_2O_3-Supported WGS Catalysts

SEM analysis indicated that the average particulate size of alumina-supported catalysts was about 30-50 nm (Figure 6).

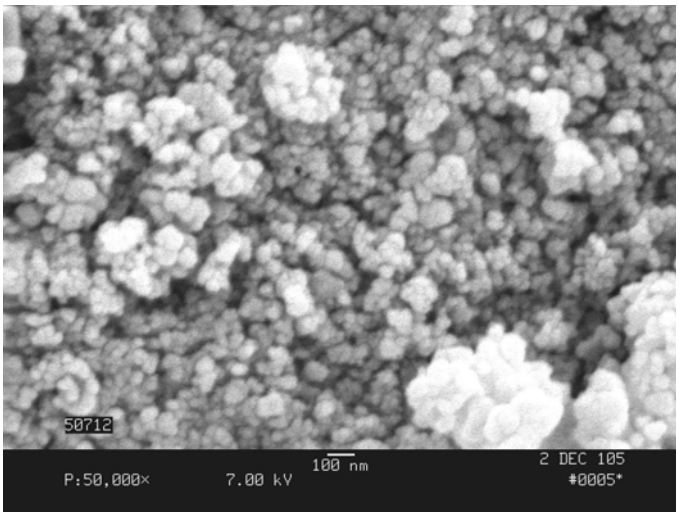

Figure 6: SEM Image of MCP Catalyst

3.3. CATALYST TESTING

The activity and stability of the WGS catalysts was evaluated using a custom-fabricated, bench-scale, high-pressure reaction system. A schematic of the testing setup is provided in Figure 7. The primary components of the test system were a stainless steel packed bed reactor, a ceramic heater, a temperature controller, gas supply manifold, two mass flow controllers (MFC), a high-pressure liquid pump, a back pressure regulator (BPR), a water trap, and a gas chromatograph (GC). Tests were conducted at different reaction space velocities by using tubular reactors of different sizes (½"OD by 6" long, ½"OD by 3" long).

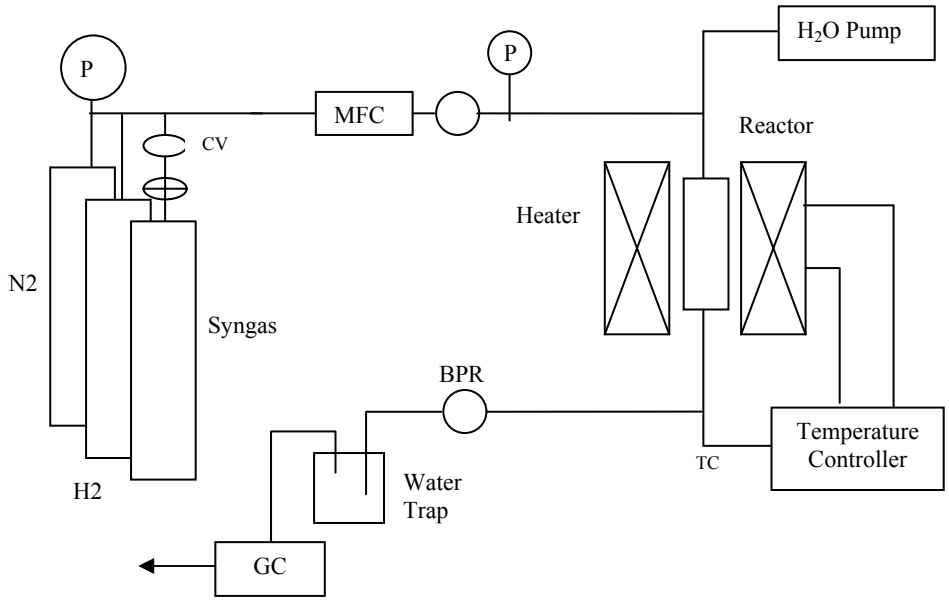

Figure 7: Schematic of Bench-Scale WGS Catalyst Testing Setup

A Varian 3800 GC equipped with a thermal conductivity detector (TCD) was used for analysis of the H_2, CO, CO_2, and CH_4 content of the reaction product. CO conversion was calculated as:

$$CO\ Conversion\ (\%) = (1 - \frac{Effluent\ CO\ Flow\ Rate}{Feed\ CO\ Flow\ Rate}) \times 100$$

Dry syngas containing approximately 25% H_2, 60% CO, 10% CO_2, 5% N_2 and 3000 ppm H_2S was used as the standard feed stream. H_2O/C molar ratios were generally maintained between 1 and 4. Chlorine was added in long-term stability tests as 350-400 ppm HCl on a dry gas basis.

The standard procedures to carry out a WGS test were as follows:

- Load and connect the reactor to the test stand
- Activate the catalyst
- Adjust temperature to desired setting while under protective atmosphere (if needed)
- Pressurize the system with flowing N_2
- Preheat H_2O evaporation line to approximately 300ºC
- Switch from N_2 to syngas at the same pressure
- Introduce steam

- Stabilize and sample

After activation, catalyst CC/Al_2O_3 was tested at space velocities of 500, 1000, and 1500 h^{-1} (dry gas-based) to identify an appropriate condition for catalyst screening (Figure 8). Conditions that achieved CO conversions well below equilibrium levels were identified for subsequent screening tests.

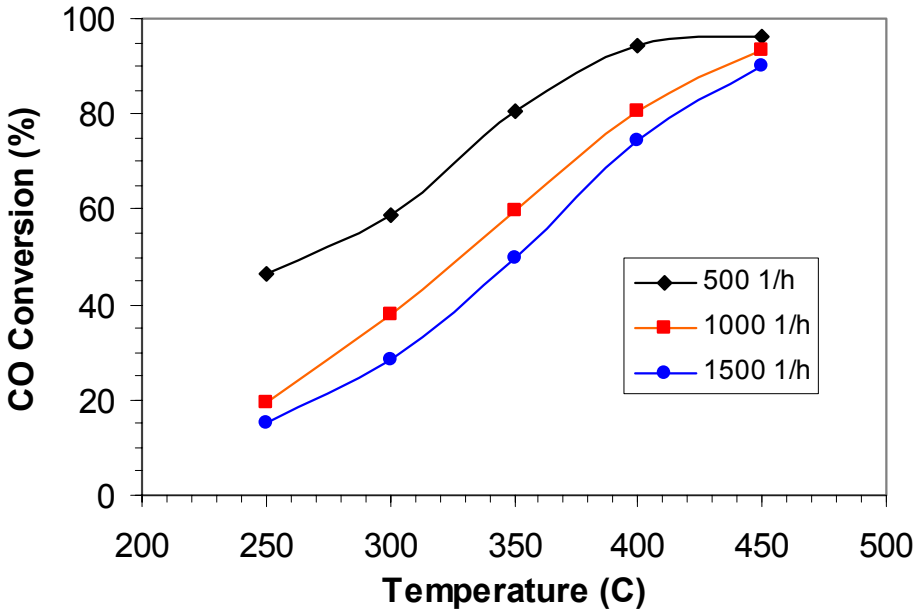

Figure 8: CO Conversion over CC/Al_2O_3 Catalysts at Three Space Velocities
(25% H_2, 60% CO, 10% CO_2, 5% N_2, 3000 ppm H_2S; H_2O/CO=3.5; Press.=400 psig)

CO conversion over CC/Al_2O_3 increased with temperature and higher conversions were obtained at lower space velocities. At temperatures below 450ºC, equilibrium conversions were not reached. GC analysis of reactor effluent gas stream showed that methanation reaction did not take place (no CH_4 was detected), indicating that the catalyst was highly selective towards the WGS reaction.

The short-term stability of the CC/Al_2O_3 catalyst was examined over the course of 21 hours. As shown in Figure 9, stable H_2, CO_2, CO and N_2 concentrations and CO conversion were obtained. There were no signs of catalyst deactivation over the 21 hour period.

All of the catalysts listed in Table III were screened under identical conditions in order to identify the most active WGS catalyst for further optimization of catalyst composition and operating conditions. Temperatures of 300, 350, 400, 450, and 500ºC, a pressure of 400 psig, and a gas hourly space velocity of 3000 h^{-1} were used. The reaction was operated at a sufficiently high space velocity so that the reaction was generally not limited by equilibrium conversions.

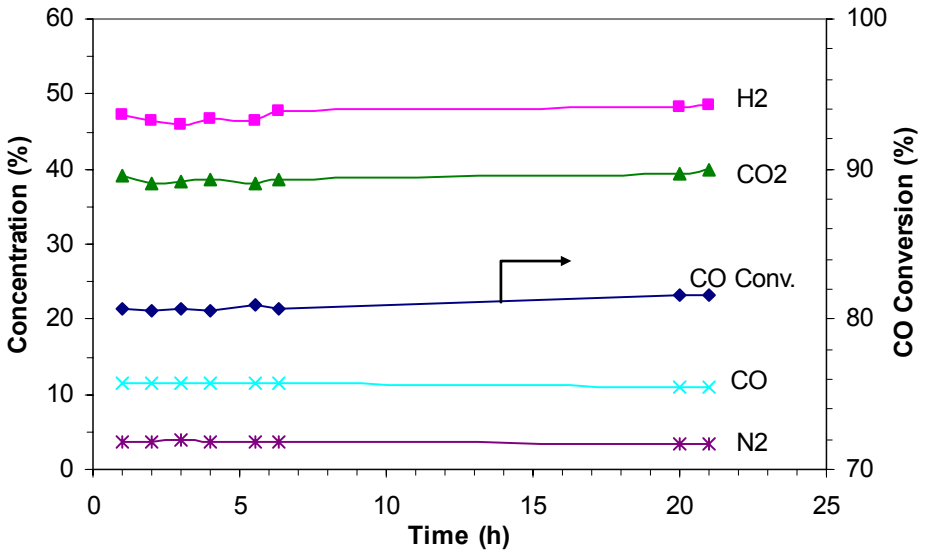

Figure 9: H_2, CO_2, CO and N_2 Concentrations and CO Conversion over CC/Al_2O_3 Catalyst
(25% H_2, 60% CO, 10% CO_2, 5% N_2, 3000 ppm H_2S; H_2O/CO=4; Temp.=350°C; Press.=400 psig; GHSV=500 h^{-1})

Figure 10 presents CO conversions for some of the catalysts tested. The two commercial WGS catalysts are labeled C1 and C2. Of all the catalysts tested, the custom-synthesized MCP catalyst was most active in the presence of 3000 ppm H_2S, followed by C2, C1 and M/Al_2O_3. Equilibrium CO conversion was approached by the MCP and C2 catalysts. MC and CC/Al_2O_3 materials were inferior at all temperatures examined. Supported catalysts were typically more active than unsupported ones and were physically stronger to withstand the harsh operating conditions. None of the catalysts exhibited measurable methanation activity.

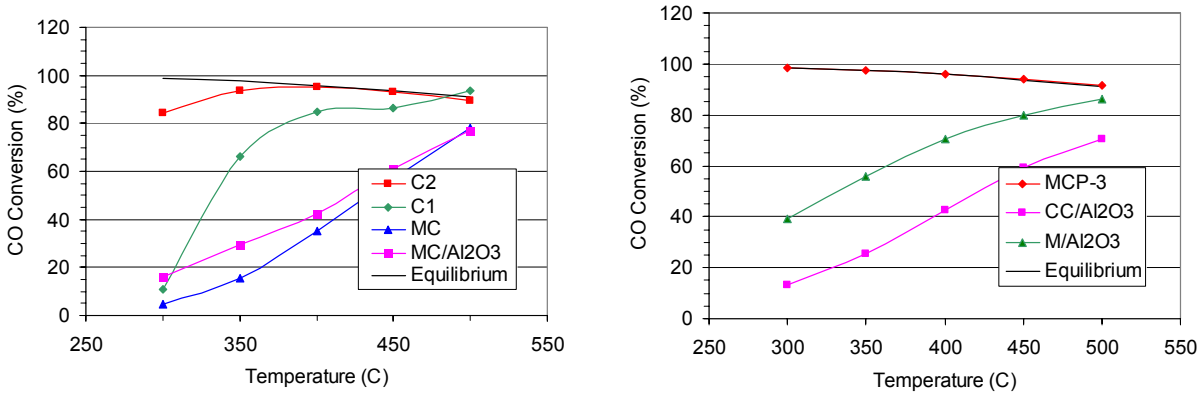

Figure 10: CO Conversion over In-House Prepared and Commercial Catalysts
(25% H_2, 60% CO, 10% CO_2, 5% N_2, 3000 ppm H_2S; H_2O/CO=4.0; Press.=400 psig; GHSV=3000 h^{-1})

Figure 11 compares the CO conversion obtained over the most active catalyst, MCP-3, with that of the commercial catalyst C2. Both catalysts were highly active at temperatures greater than 400ºC. However, at temperatures below 400 ºC, MCP-3 was clearly more active, demonstrating that it was effective in a wider temperature range from 300 to 500ºC. Because of the superior performance of the MCP-3 catalyst, later studies were focused on the MCP series catalysts.

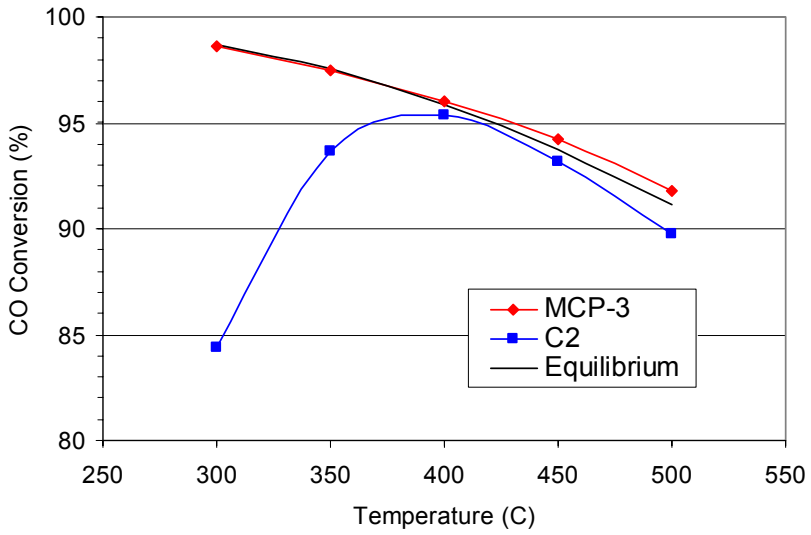

Figure 11: Comparison of CO Conversion over MCP-3 and Commercial C2 Catalysts
(25% H_2, 60% CO, 10% CO_2, 5% N_2, 3000 ppm H_2S; H_2O/CO=4.0; Press.=400 psig; GHSV=3000 h^{-1})

Additional testing of the MCP series catalysts was conducted to examine the effects of other operating parameters on catalyst performance. An increase in space velocity from 3000 to 12,000 h^{-1} resulted in a decrease in CO conversion from 98% to 82% at 400 ºC and 400 psig. At space velocities below 3000 h^{-1}, equilibrium conversion was achieved at all measured conditions.

To explore the effects of active phase loading on catalyst performance, the catalytic activity of the MCP series of catalysts was evaluated at 12,000 h^{-1} GHSV. Figure 12 shows the CO conversion measured over the three catalysts with increased metal loading from MCP-1 to MCP-3. MCP-3 was the most active catalyst tested.

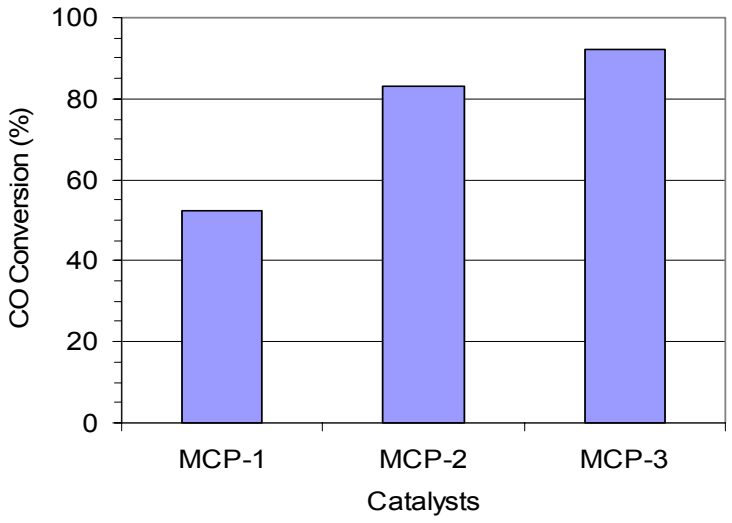

Figure 12: CO Conversion over MCP Catalysts with Different Metal Loadings
(25% H_2, 60% CO, 10% CO_2, 5% N_2, 3000 ppm H_2S; H_2O/CO=4.0; Press.=400 psig; Temp.=400ºC; GHSV=12,000 h^{-1})

The long term effects of catalyst exposure to high concentrations of H_2S and HCl were evaluated. Several catalysts were tested at 3000 h^{-1} space velocity in the presence of 3000 ppm H_2S and 350 ppm HCl. Figure 13 is the result of one particular 200 hour test with catalyst MCP-3. The initial feed syngas mixture contained 3000 ppm H_2S, but no chlorides. After the catalyst had displayed stable performance for over 50 hours, it was challenged by the addition of 350 ppm HCl. There was some initial loss of catalyst activity, from 97% CO conversion down to about 80%. But the CO conversion stabilized at 80% after 50 hours. After the system was exposed to HCl for over 100 hours, HCl was removed from the feedstock. The performance then proceeded to recover to almost the initial value, demonstrating that the deteriorative effect of HCl was reversible.

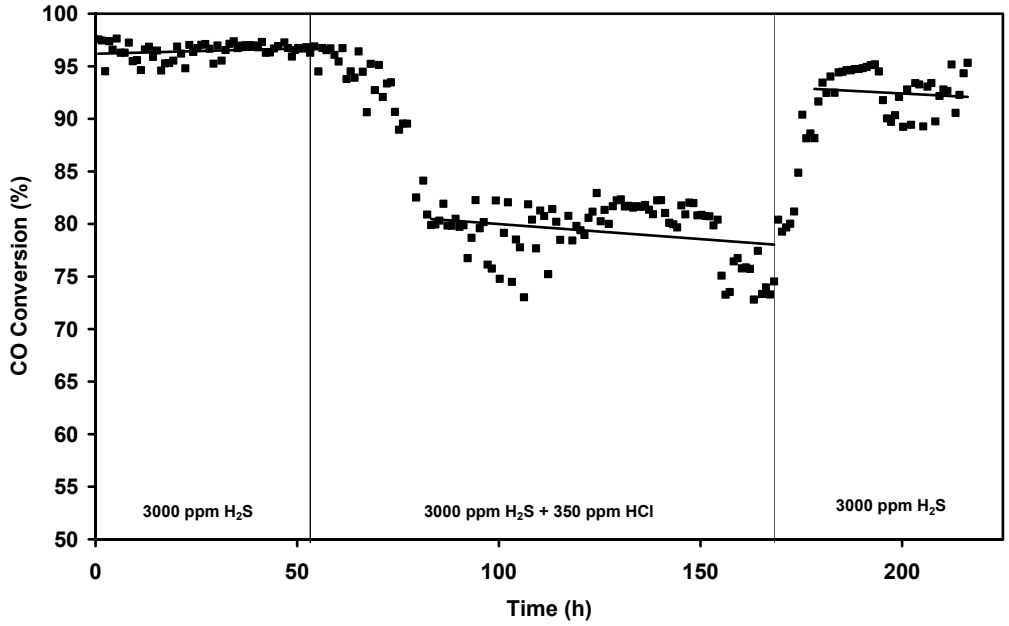

Figure 13: CO Conversion over MCP-3 Catalyst for Extended Duration
(25% H_2, 60% CO, 10% CO_2, 5% N_2, 3000 ppm H_2S, (350 ppm HCl); H_2O/CO=4.0-4.5; Press.=400 psig; Temp.=400°C; GHSV=3000 h^{-1})

4. HYDROGEN PERMEABLE MEMBRANE DEVELOPMENT

The H_2-permeable membranes developed in this program are based upon Group V metals. Group V metals have a body centered cubic crystalline structure that exhibit greater H permeability than Pd (Figure 14). However, Group V metals are more reactive, more susceptible to H_2 embrittlement than Pd and do not catalyze the dissociation and association of H_2 molecules as effectively as Pd.

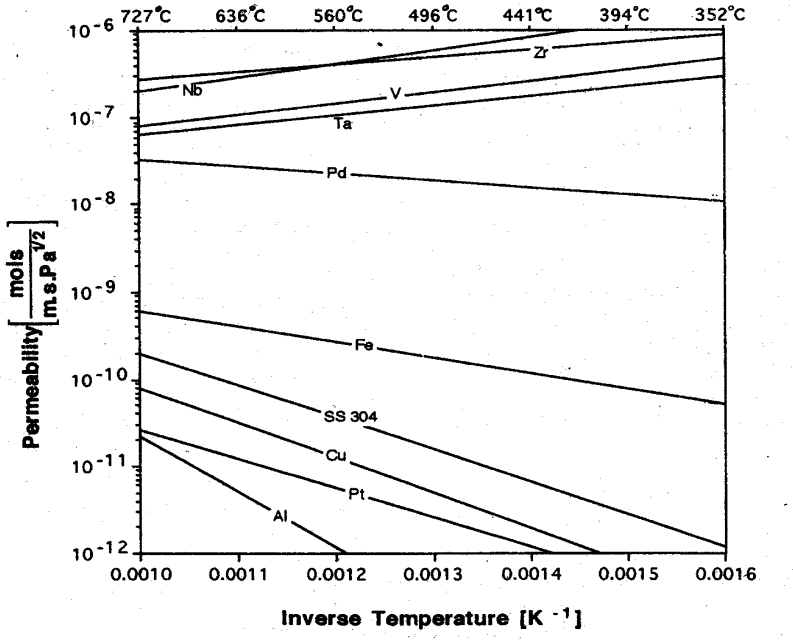

Figure 14: Hydrogen Permeability Derived from Diffusivity and Solubility[2]

To overcome this shortcoming, a layered membrane structure was employed to efficiently transport H_2 from one side of the dense membrane to the other (Figure 15). The membrane consists of a dense Group V metal core, coated with materials that catalyze the dissociation and association of H_2. This configuration offers a lot of design flexibility because the material that dissociates H_2 from the contaminant-laden coal gas, does not need to possess high H permeability, while the underlying Group V substrate only needs to permeate H and does not need to have high catalytic activity or contaminant tolerance.

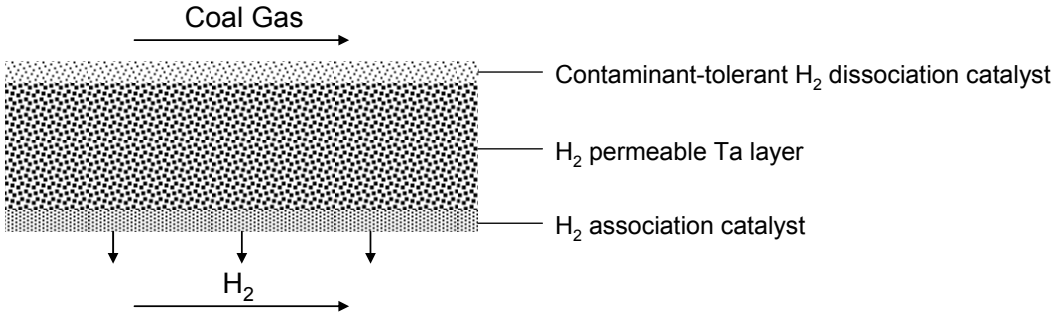

Figure 15: H_2-Permeable Membrane Schematic

The potential advantages that the layered membrane approach has over Pd-based membranes include:

- No requirement to remove S and Cl contaminants – through proper selection of the dissociation catalyst composition, complete sulfur and halide tolerance may be imparted to the membrane.
- Able to withstand high transmembrane pressure – the membrane can be thicker and still achieve adequate flux due to the order of magnitude increase in permeability over Pd
- Low-cost – due to reduced precious metals content

4.1. MEMBRANE PREPARATION

To simplify membrane sealing challenges, a tubular membrane geometry was employed during the membrane development process. Tantalum tubes with diameters of 3/8" and 1/4" and wall thicknesses of 0.38, 0.51 and 0.76 mm were used.

Electroless plating was selected as a means to deposit the desired catalyst compositions onto the surface of the tubes. Pd, Pd alloy and Pd-free catalysts were examined. Prior to plating, the Ta tubes were typically cleaned by mechanically sanding the external surface followed by rinsing with an acidic solution to remove residual oxide species.

The electroless plating process for palladium requires that the surface be properly activated beforehand. Surface activation was carried out by sequentially immersing clean tubular substrates in an aqueous bath containing tin (II) chloride as a reducing agent and a second aqueous bath containing palladium (II) chloride. Table IV presents the typical compositions of activating and plating solutions.

Table IV: Activating and Plating Solutions

Activation Solutions				
Tin Chloride Solution			Palladium Salt Solution	
$SnCl_2$	1 g/L		$PdCl_2$	0.1 g/L
HCl (37%)	1 mL/L		HCl (37%)	1 mL/L
Temperature	25 °C		Temperature	25 °C
Plating Solutions				
$PdCl_2$			4.05 g/L	
EDTA 2Na			40.0 g/L	
NH_4OH			290 mL/L	
N_2H_4			7.5 mL/L	
pH			11	
Temperature			55 °C	

During activation, the tube was immersed into the tin bath for 5 minutes. After withdrawing from the tin bath, excess solution was removed and the tube was rinsed gently with deionized water. The tube was then dipped into the Pd bath for 5 minutes, rinsed in 0.01 M HCl solution and in deionized water. The above steps were repeated 5 times and the tube was finally dried at room temperature, followed by 110ºC for 1 hour.

After the activation procedure, the tube was prepared for catalyst plating by isolating the surface to be plated. In all membranes prepared in this program, the Pd and alloy coatings (2-8 micron) were deposited on the outer surface of the tube while a thin layer of Pd (typically ~1 micron) was deposited on the internal surface of the tube.

Electroless plating rates were established by conducting a series of Pd and alloy metal plating tests on each surface of the substrate tubes at fixed conditions. Pd and alloy metal uptake amounts were obtained as a function of plating time. As shown in Figure 16, when a constant amount of reducing agent was added to the plating solution, linear relationships were obtained for Pd plating on the inner surface and for the alloy metal on the outer surface. For Pd plating on the outer surface, the plating rate decreased after about two hours. The plating of the alloy metal was slower than that of palladium.

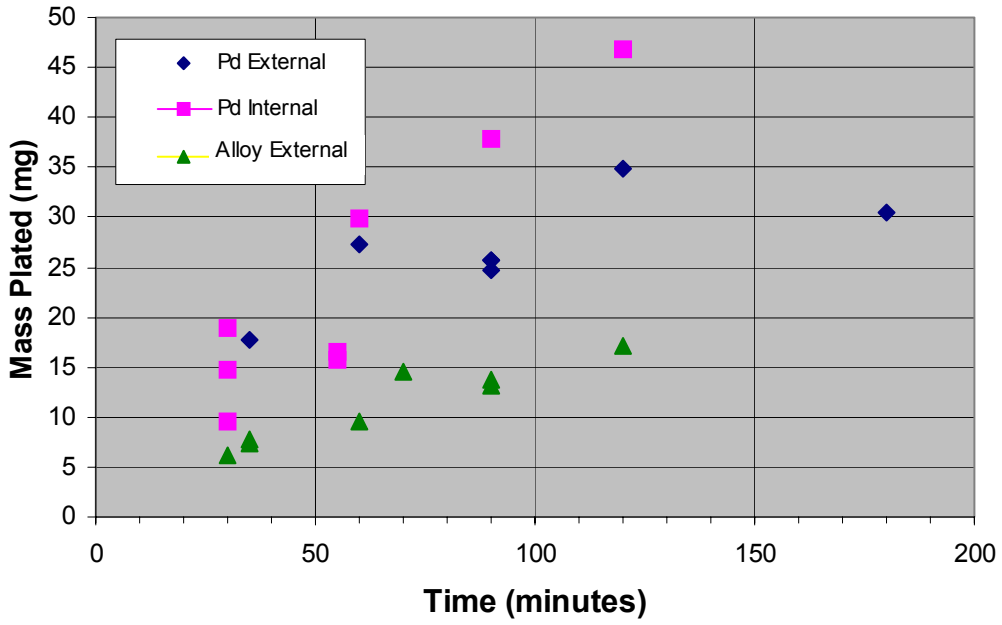

Figure 16: Relationship between Mass of Metal Plated and Plating Time

Following the electroless plating step, the tubes were heat-treated in argon to fully alloy the coated metals. The atmosphere inside the tube furnace was purged with high purity argon for one hour before the heating ramp was started. Soaks at 400, 500, and 600°C with a ramp rate of 1°C/minute were commonly used. Photographs of the cleaned tantalum substrate and coated membrane tubes are provided in Figure 17.

Figure 17: Ta Substrate and Coated Membrane Tubes

Over the course of the program, 75 membrane samples were prepared and characterized. Initial efforts focused on Pd catalytic coatings in order to baseline the technology, while the majority of the effort ultimately studied Pd-alloy catalytic coatings.

4.2. MEMBRANE CHARACTERIZATION & TESTING

The H_2 permeability and stability of membranes were evaluated in a custom-fabricated, bench-scale, gas permeation test system. A schematic of the permeation test stand is provided in Figure 18. It consisted of a stainless steel membrane housing, a ceramic heater, a temperature controller, two mass flow controllers (MFC), two back pressure regulators (BPR), and valves and fittings. For initial testing, a H_2/He (95%/5% by volume) mixture was fed onto the outer surface of the membrane. H_2 permeated through the membrane, and was blended with N_2 for GC analysis. In most tests, the H_2 partial pressure on the low pressure side of the membrane was maintained at 1 atm.

To secure the tubular membrane in the membrane housing, a stainless steel insert was inserted into each end of the membrane tube to support the membrane. Stainless steel compression fittings were used to connect one end of the membrane tube to the permeate exit tubing and to seal the other end with a plug. Permeate effluent was analyzed for He, H_2 and N_2 by the Varian GC to check for cross membrane leaks and to determine the permeability of the membrane.

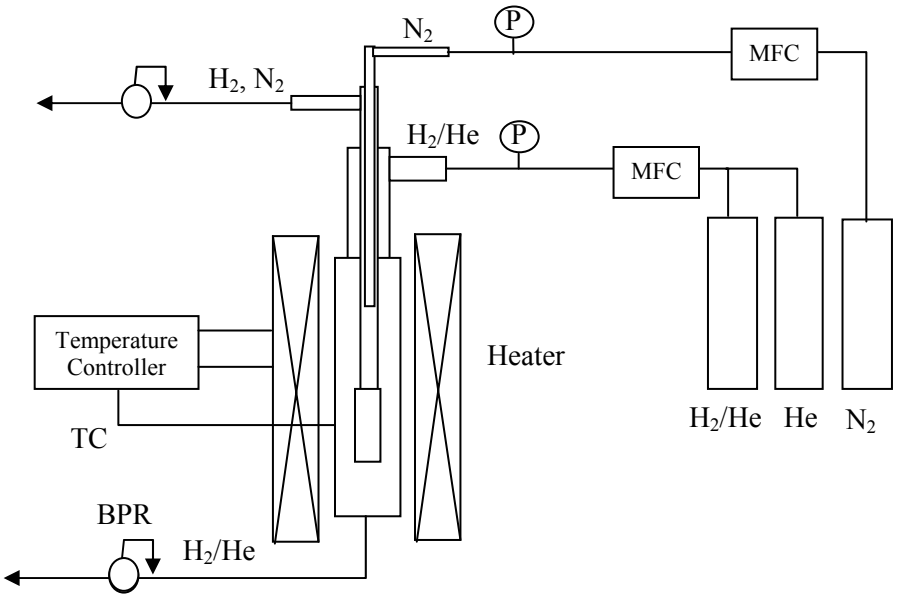

Figure 18: Schematic of Bench-Scale WGS Catalyst Testing Setup

Selected membranes, with and without catalyst coatings, were characterized by XRD, SEM, energy dispersive X-ray analysis (EDX), and Auger electron spectroscopy (AES) to characterize crystalline phases, composition and microstructure. XRD analysis were carried out with a Rigaku D/MAX-B X-ray diffractometer with a Cu anode. AES analyses were carried out with a PEI 670 Auger Microprobe system.

The surface view of a typical coated tubular membrane is presented in Figure 19. The catalyst coating on the as-prepared membrane was generally uniform and consisted of grains of about 2 microns in diameter. Although the coated surface was fairly uniform, there were small microcracks in the coating through which the underlying substrate could be exposed. Good coating adhesion was generally observed, with delamination of the coating from the substrate only observed in samples that were not subjected to proper surface treatment and cleaning.

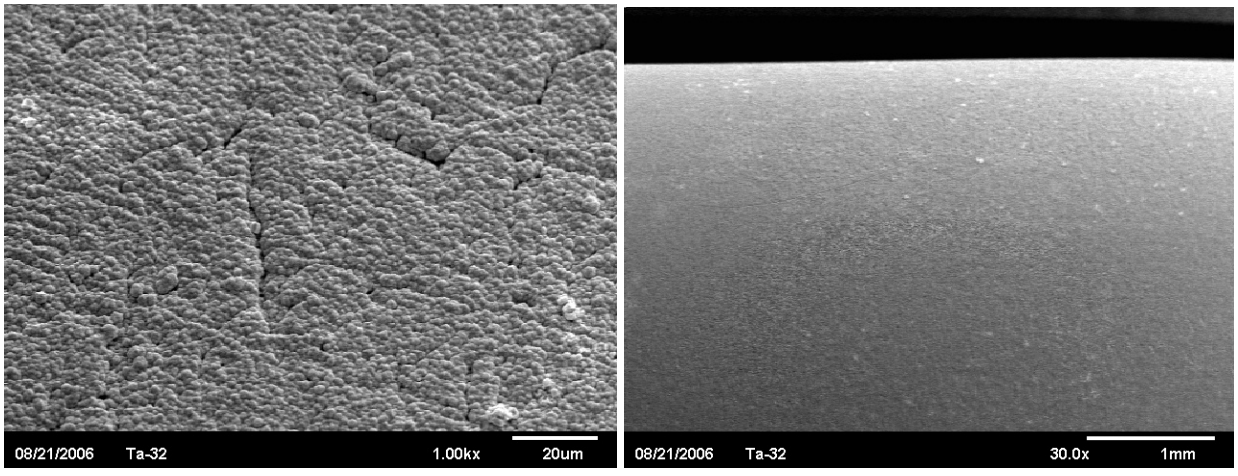

Figure 19: SEM Image of an As-Prepared Membrane

Figure 20 shows a cross-sectional view of a tested membrane following fracture. The dense Ta substrate is located on the left side of the image and the catalyst coating is observable on the right edge. The catalyst coating layer is about 2 microns thick in this sample.

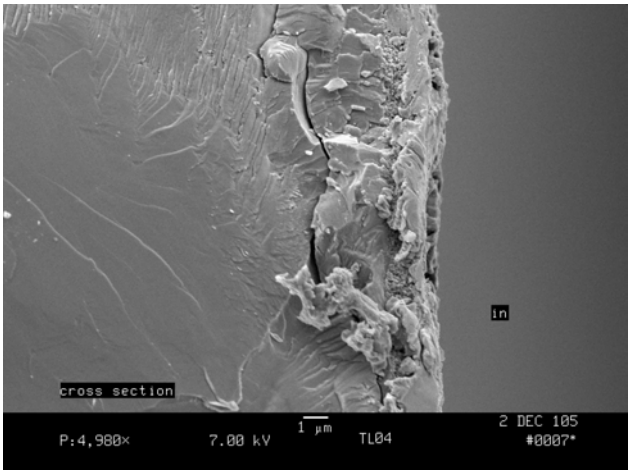

Figure 20: Cross-section SEM of a Tested Membrane

The H_2 permeabilities of the initial membranes produced in this program were measured to evaluate the effects of membrane thickness, catalyst coating technique, catalyst composition and operating conditions on their H_2 permeability.

As expected, a catalytic coating was required to achieve appreciable H_2 permeation through the tantalum layer (Table V). However, catalyst coated membranes were more prone to mechanical failure due to hydrogen embrittlement below 350°C than uncoated tubes.

Table V: Effect of Catalyst Coating on H_2 Permeability at 200 psi H_2 Pressure

Temperature (ºC)	H_2 Permeability (1E-8, mol/s/m/$Pa^{0.5}$)	
	No Catalyst	With Pd Catalyst
300	0.00	not measured
400	0.03	0.92
500	0.31	1.64

The dependence of H_2 flux on transmembrane H_2 partial pressure is shown in Figure 21 for a thick wall membrane tested at 500ºC. The membrane was operated over a wide range of transmembrane H_2 pressures from 0 to 200 psi. For a WGS membrane reactor operated at near equilibrium conditions (*i.e.*, 50% H_2 content), this corresponds to roughly 0 to 400 psi in total pressure. The H_2 flux is approximately proportional to square root of H_2 partial pressure, consistent with diffusion of hydrogen atoms through the tantalum membrane substrate being the rate limiting step.

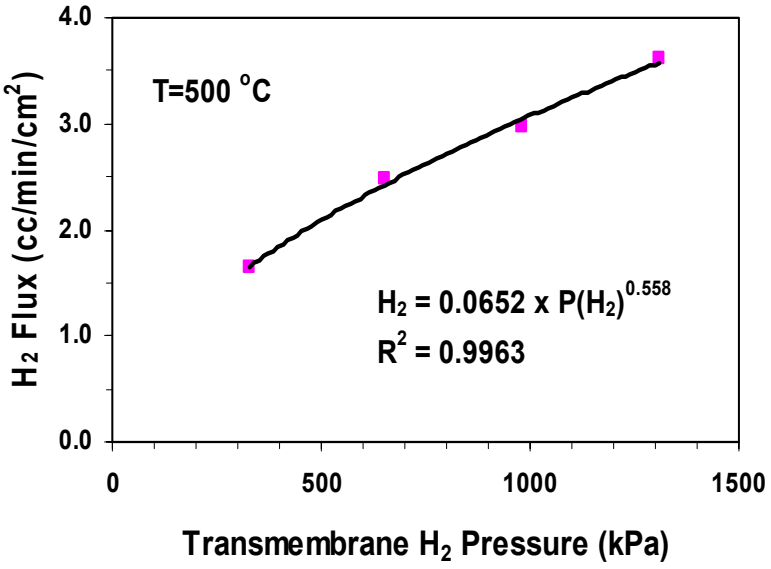

Figure 21: Dependence of H_2 Flux on Transmembrane H_2 Partial Pressure at 500°C

Membrane preparation variables that were subsequently examined included tubular substrate diameter, tubular substrate wall thickness, alloy catalytic coating composition, alloy catalytic coating thickness and membrane annealing time.

The effect of annealing conditions on membrane morphology and performance were examined by varying membrane annealing time and temperature. Annealing temperatures ranging from 400 to 600°C were examined at annealing times of 5 to 18 hours. While longer annealing times resulted in smoother catalyst coating with fewer surface details (Figure 22), they did not have any measurable effect on membrane permeability. Lower annealing temperatures yielded higher permeabilities due to presumably reduced intermetallic diffusion at the catalyst-substrate interface.

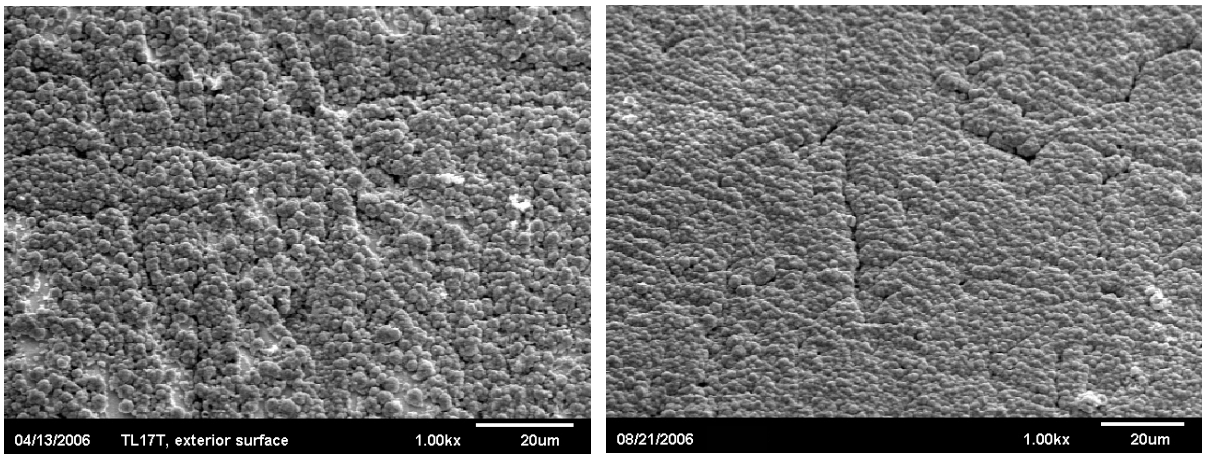

Figure 22: SEM Images of Membrane Annealed for 5 hours

Pd alloy composition was found to have a significant effect on H_2 permeability. The H_2 permeabilities of a variety of membranes tested at 425-450°C under a H_2/He environment are

presented in Figure 23. When the amount of Pd nominally present in the coating was below 65%, low membrane permeability was observed.

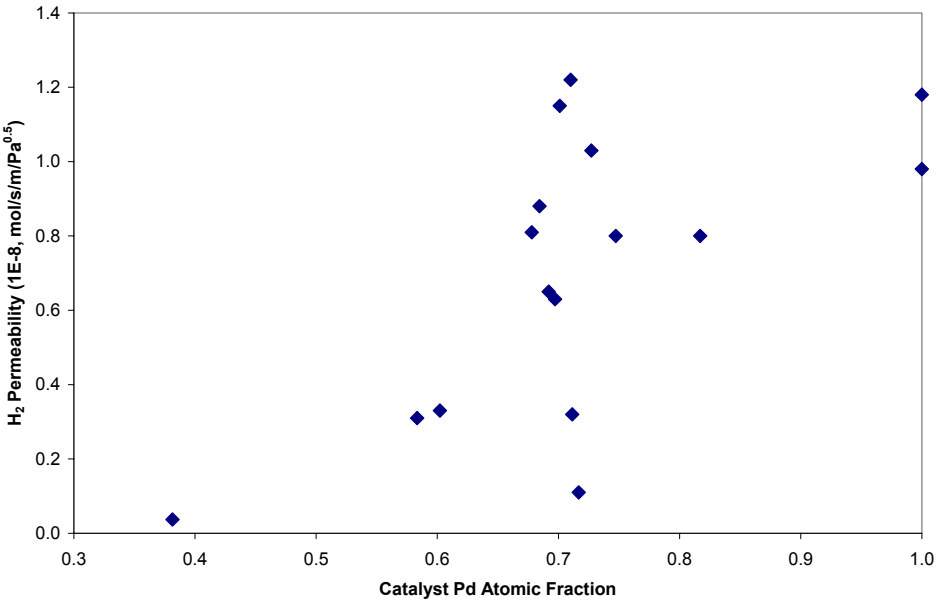

Figure 23: H_2 Permeability and Coating Composition

The effect of H_2S on H_2 permeability was also examined for a variety of membranes. Figure 24 presents a typical plot of H_2 permeability as a function of time. Following membrane stabilization in 5% He/95% H_2 for 17 hours, 2000 ppm H_2S was added to the gas mixture and the H_2 flux was monitored until the permeability stabilized. In Figure 24, the H_2 permeability decreased by 30% within 28 hours of exposure to 2000 ppm H_2S.

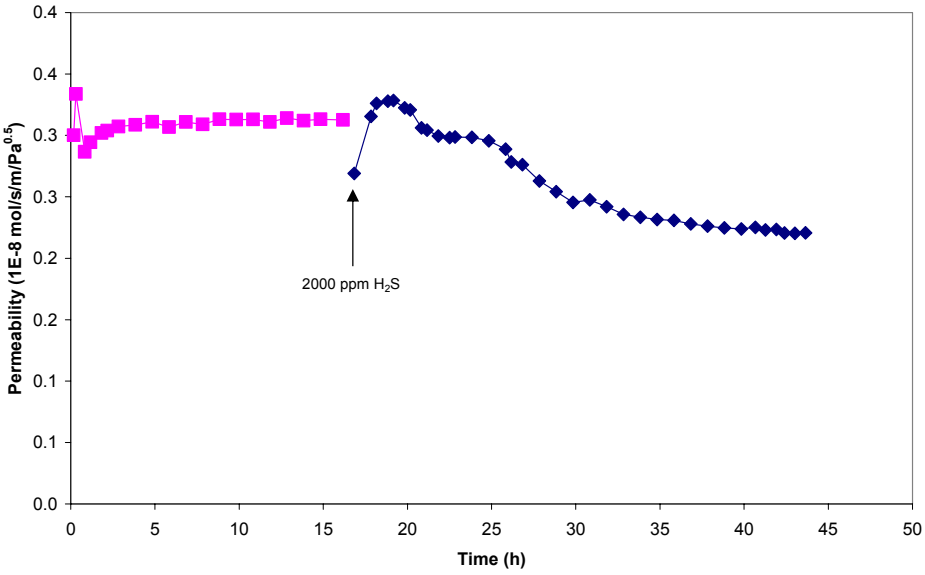

Figure 24: H_2 Permeability of Membrane Coated with 58% Pd

The Pd content of the alloy catalytic coating exhibited a significant influence on the extent to which membrane performance degraded in the presence of H_2S. Figure 25 plots the H_2 permeability retained by different alloy-coated membranes upon exposure to 2000 ppm H_2S. Membranes with coatings containing a targeted amount of 58 to 68% Pd retained greater than two thirds of their permeability upon exposure to H_2S. Maximum H_2 permeabilities were thus observed at alloy Pd concentrations between 65 and 68%.

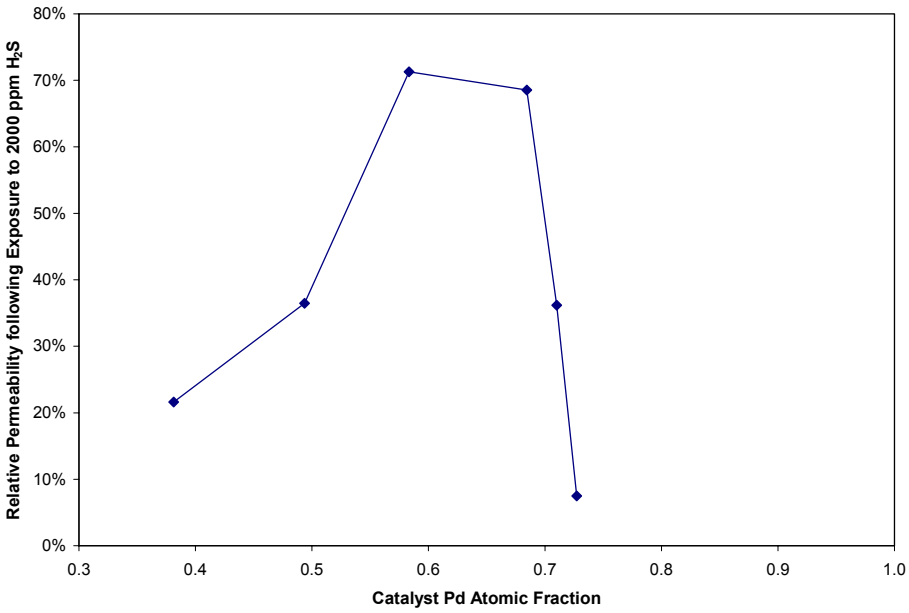

Figure 25: Effect of 2000 ppm H_2S on H_2 Permeability at 450°C

Initial testing of membrane performance in the presence of steam revealed rapid membrane degradation (Figure 26). Oxidation of the membrane substrate by H_2O was postulated as a potential degradation mechanism. SEM analysis of Membrane 40 (100% Pd, 1.5 micron coating) revealed the formation of a disruptive intermediate layer between the membrane substrate and catalytic coating following exposure to steam at 450°C.

In order to improve the stability of the membrane in moist atmospheres, changes were made to the membrane formulation and synthetic process in order to reduce imperfections in the coated catalyst layer which could allow H_2O to come in contact with the Ta membrane substrate. These changes included building up the external catalyst coating with multiple thin electroless plated layers, increasing the overall thickness of the external catalyst coating and reducing the membrane annealing temperature.

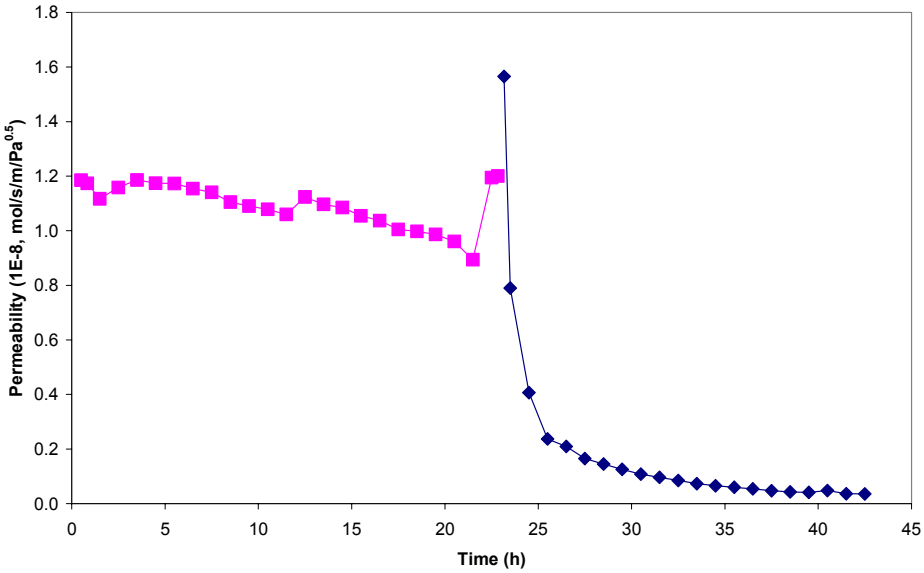

Figure 26: H_2 Permeability of Membrane 40 in the Absence and Presence of 50% Steam

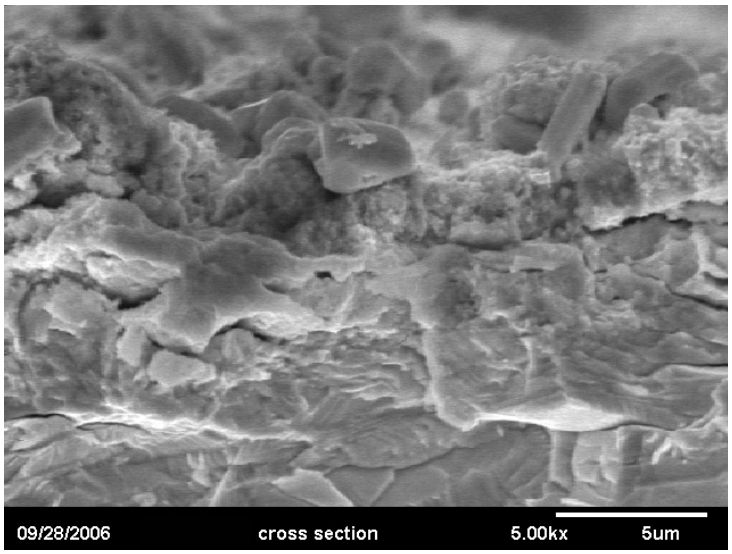

Figure 27: Scanning Electron Micrograph of Tested Membrane #40

Hydrogen permeability increased by a factor of six upon shortening the post-coating annealing time and decreasing the annealing temperature. Figure 28 presents the hydrogen permeability of membranes prepared using half the annealing time (Membrane 56) and progressively reduced annealing temperatures (Membrane 57 and 61). Reducing the annealing time increased the initial H_2 permeability of the membrane two-fold over typical previous samples. Reducing the annealing temperature resulted in five- and six-fold increases over previous samples.

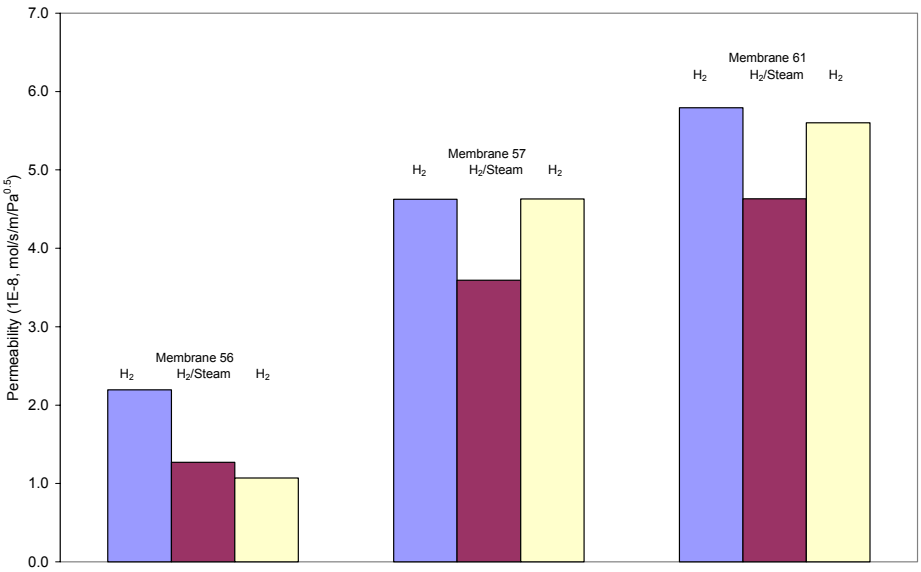

Figure 28: H_2 Permeability of Membranes in the Absence and Presence of 33% Steam

Membrane stability in the presence of water was excellent in the membrane samples produced by the modified coating technique. Membrane 57 (68% Pd alloy, 4 micron coating) exhibited a 22% reduction in permeability when exposed to a stream containing 33% water (Figure 29), while Membrane 61 (71% Pd alloy, 6 micron coating) exhibited a 20% reduction. Full recovery of initial H_2 permeabilities was realized upon removal of water from the feed stream. This indicated that the membrane structure was not significantly affected by the steam, and that the reduction in permeability may have been caused by competitive surface adsorption between H_2 and H_2O species.

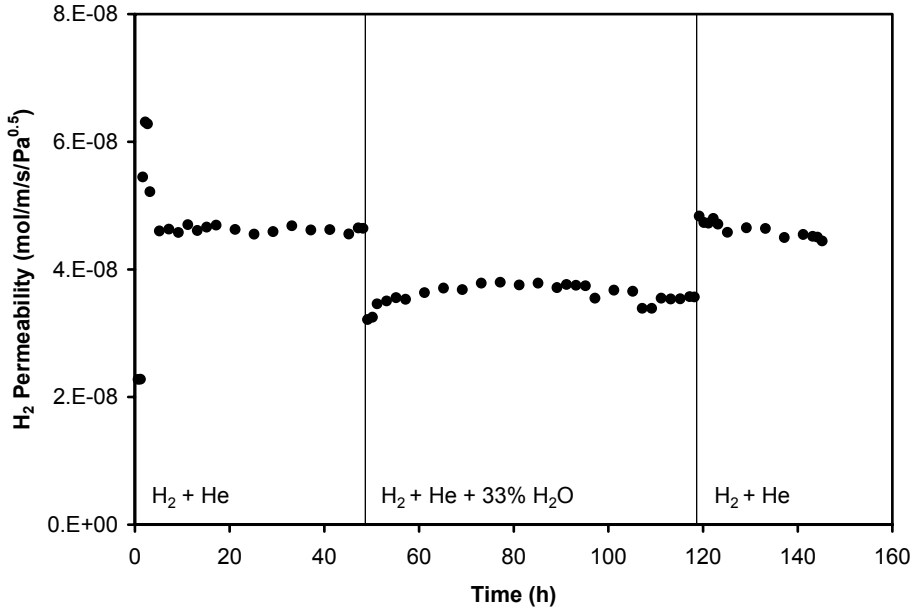

Figure 29: H_2 Permeability of Membrane 57 in the Absence and Presence of 33% Steam

The benefit of the multi-step catalyst deposition technique, independent of effects of coating thickness, is presented in Figure 31. The two membranes in the figure contain the same catalyst alloy coated at a thickness of 4 microns. In one, the alloy was deposited through multiple coatings, in the other, the alloy was deposited in a single layer. The hydrogen permeability of the multiple-layered membrane was higher and more stable than that of a single-layered membrane.

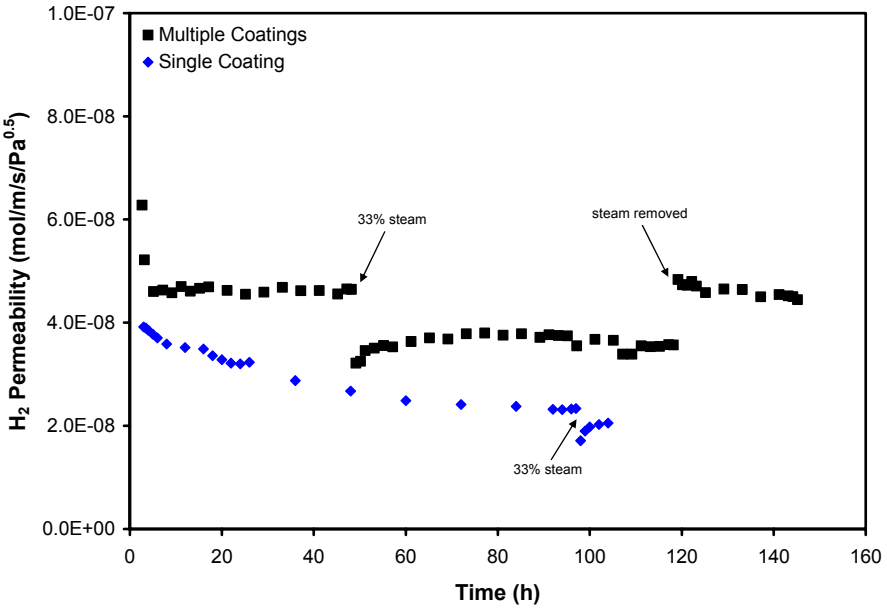

Figure 30: Effect of Coating Procedure on Membrane Permeability

The permeabilities of several promising membranes are presented in Figure 31 relative to the permeability of Pd and Ta. The permeability of these membranes is several times greater than that of Pd membranes and is in line with previously reported permeabilities of Ta, which were generally determined with thicker tantalum membranes.

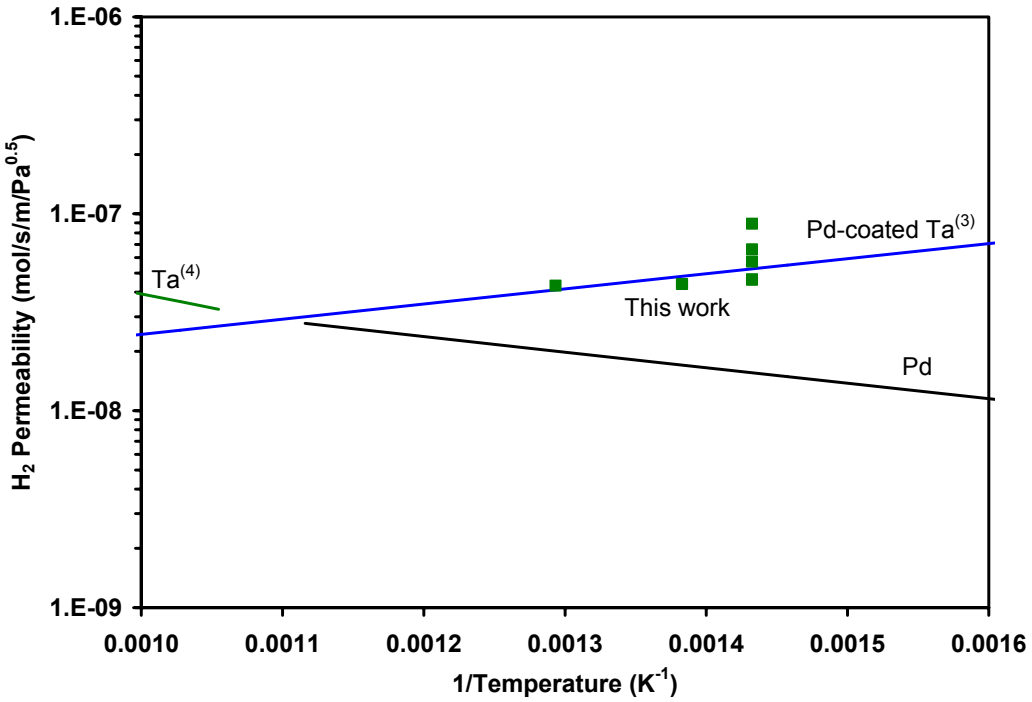

Figure 31: H_2 Permeability of Pd, Ta and Subject Samples[3,4]

The effect of temperature on H_2 permeability and membrane stability was studied with Membrane 58 (69% Pd alloy, 6 micron coating). Measurements were taken at 425, 450, 500, 425 and then 400°C. An increase in permeability at 450°C was followed by a decrease in permeability upon heating to 500°C. Upon returning to 425°C, a loss in permeability was observed, presumably due to membrane annealing that took place at the extended testing time spent at 500°C. A subsequent decrease in permeability was observed at 400°C.

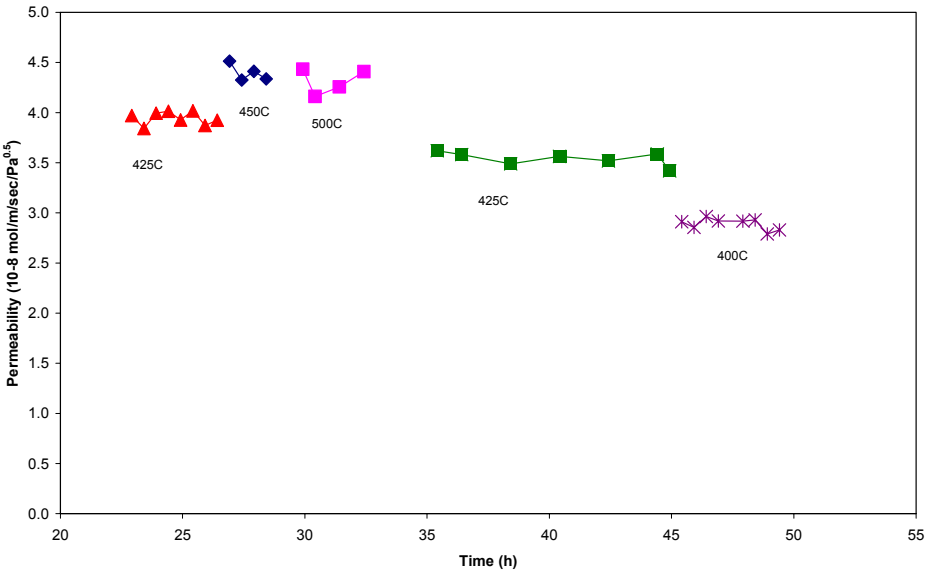

Figure 32: Temperature Effects on H_2 Permeability of Membrane 58

The effect of H_2S on H_2 permeability was examined for a variety of membranes. Figure 33 presents a plot of H_2 permeability as a function of time for Membrane 58, which was one of the more sulfur-tolerant formulations. Following membrane stabilization in 5% He/95% H_2 for five hours, 2000 ppm H_2S was added to the gas mixture and the H_2 flux was monitored until the permeability stabilized. In this case, the permeability was stable through twenty hours of H_2S exposure and only decreased by 10% from the value observed in the absence of sulfur. No recovery in H_2 permeability was observed upon removal of sulfur from the test stream.

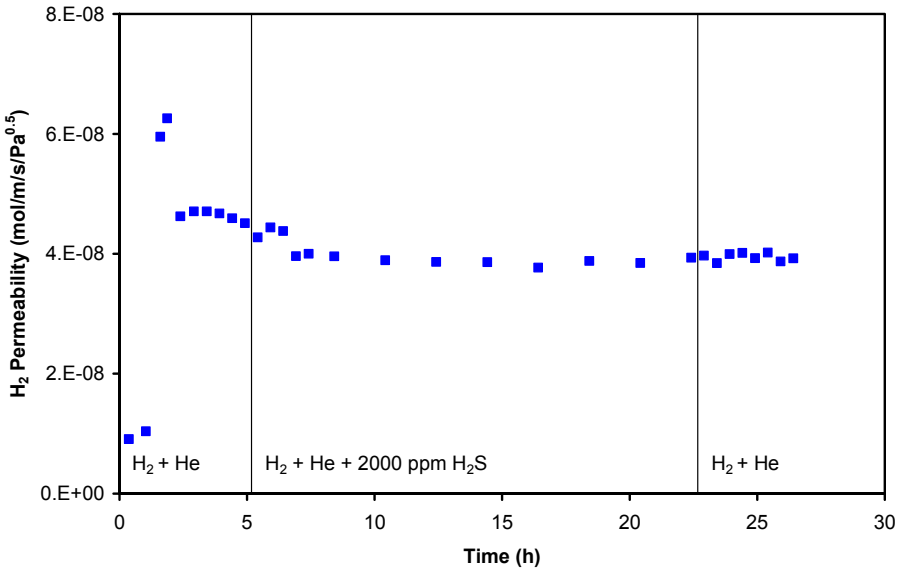

Figure 33: H_2 Permeability of Membrane 58 in the Presence of H_2S

In an effort to better understand what membrane characteristics lead to high permeability and resistance to poisoning by sulfur, detailed compositional and microstructural analyses of four membranes with different H_2 permeation abilities were conducted. Several properties of these membranes are summarized in Table VI. Membranes 58 and 70 exhibited high H_2 permeability and excellent tolerance of H_2S. Membrane 61 exhibited high permeability, but poor H_2S tolerance. Membrane 72 exhibited poor permeability and poor tolerance of H_2S.

Table VI: Properties of Selected Membranes

Membrane ID	Nominal Pd Content (%)	External Coating Thickness (micron)	Pure H_2 Permeability (mol/m/s/$Pa^{0.5}$)	Permeability Decrease in 2000 ppm H_2S (%)
58	69	6	$4.5x10^{-8}$	14
70	63	3	$7.0x10^{-8}$	10
61	71	6	$5.6x10^{-8}$	65
72	64	3	$1.4x10^{-8}$	>90

SEM images of the surfaces of Membranes 70 and 72 following exposure to H_2 and H_2S at 425°C are presented in Figure 34. The surface morphology of Membrane 70 was similar to that of Membranes 58 and 61 and consisted of 2-4 micron diameter grains. The coating of Membrane 72 was slightly different, consisting of smaller, less well-defined grains.

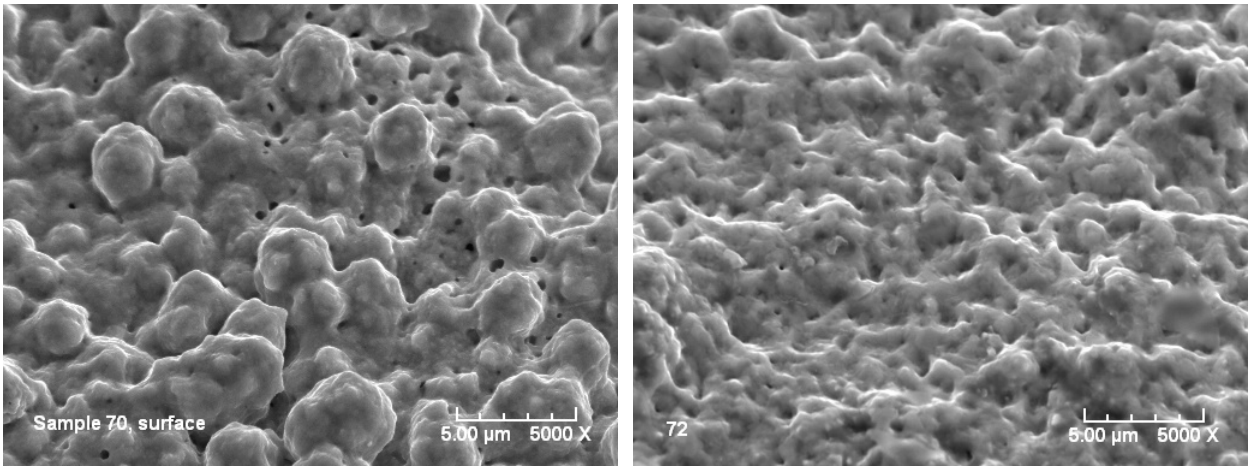

Figure 34: SEM Images of Membrane 70 and 72 Surfaces

Energy dispersive X-ray (EDX) analysis of several membranes following permeation testing was conducted to characterize membrane structure and composition. SEM and EDX images of Membranes 58, 70 and 61 following permeation testing are presented in Figure 35, Figure 36, Figure 37, and Figure 38. Of the four membranes, only Membrane 58 possessed detectable amounts of sulfur on the surface. Surface Pd and S dot maps of Membrane 58 exhibited differences in shading (Figure 35), and thus different localized Pd/S elemental ratios. However, in cross section (Figure 36), it was apparent that the S is present throughout the thickness of the catalytic coating.

Figure 37 presents elemental mapping of Membrane 70 in cross-section. A clear delineation between the Ta substrate and the Pd alloy catalytic coating was evident. The thickness of the coating in the Pd dot map image was 2.5 microns, in good agreement with the calculated coating thickness of 3 microns based upon observed membrane weight changes during the electroless plating process. A micron-sized void was present in the Ta substrate, slightly below the interface of the substrate and coating. No significant interdiffusion of Ta and Pd was evident.

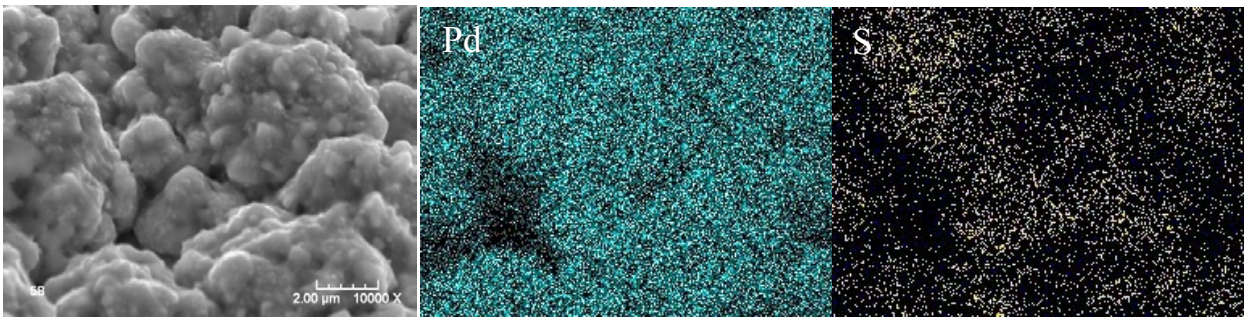

Figure 35: SEM and EDX Images of Membrane 58 Surface

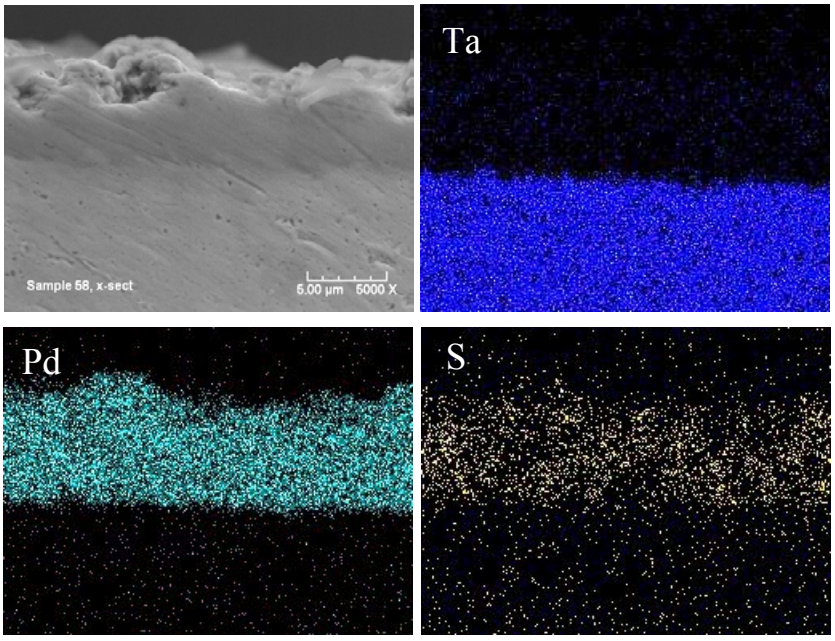

Figure 36: SEM and EDX Images of Membrane 58 Cross Section

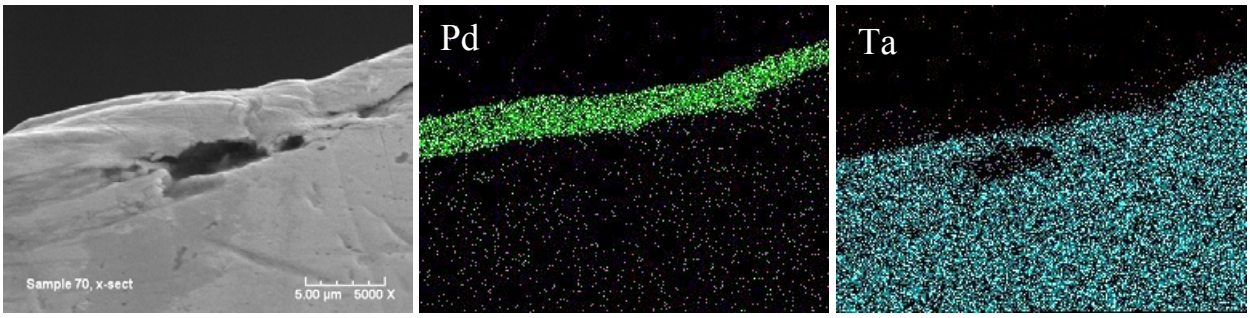

Figure 37: SEM and EDX Images of Membrane 70 Cross-Section

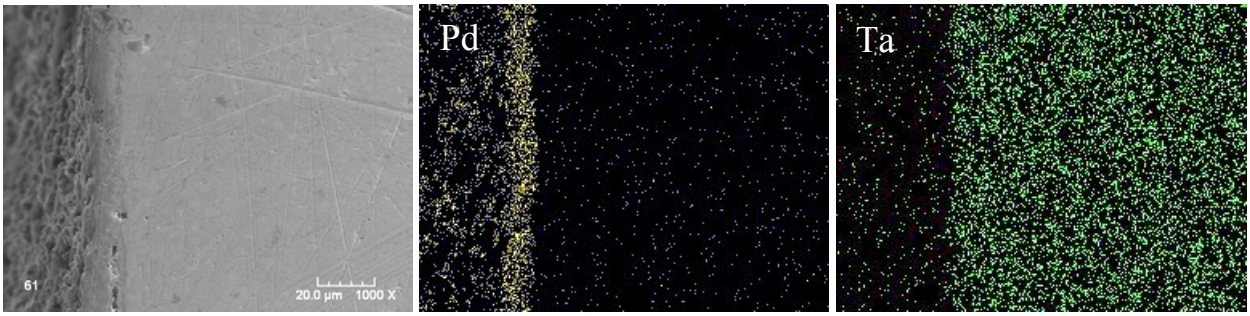

Figure 38: SEM and EDX Images of Membrane 61 Cross-Section

Figure 38 provides images of Membrane 61 in cross-section. The catalyst coating thickness was approximately 8 microns in these images.

XRD analysis of used membranes was conducted to identify crystalline phases present in the catalytic coating. Powder XRD scans for Membranes 70, 61 and 72 are presented in Figure 39. Membrane 70 (and 58, not shown) exhibited peaks attributable to a face centered cubic (fcc) Pd

alloy and to Pd_4S. The catalyst coating of Membrane 61 was also comprised of a fcc Pd alloy, but much lesser amounts of Pd_4S. Membrane 72 was comprised of a mixture of fcc Pd alloy and a body center cubic (bcc) Pd alloy. No crystalline sulfide phases were observed in membrane 72.

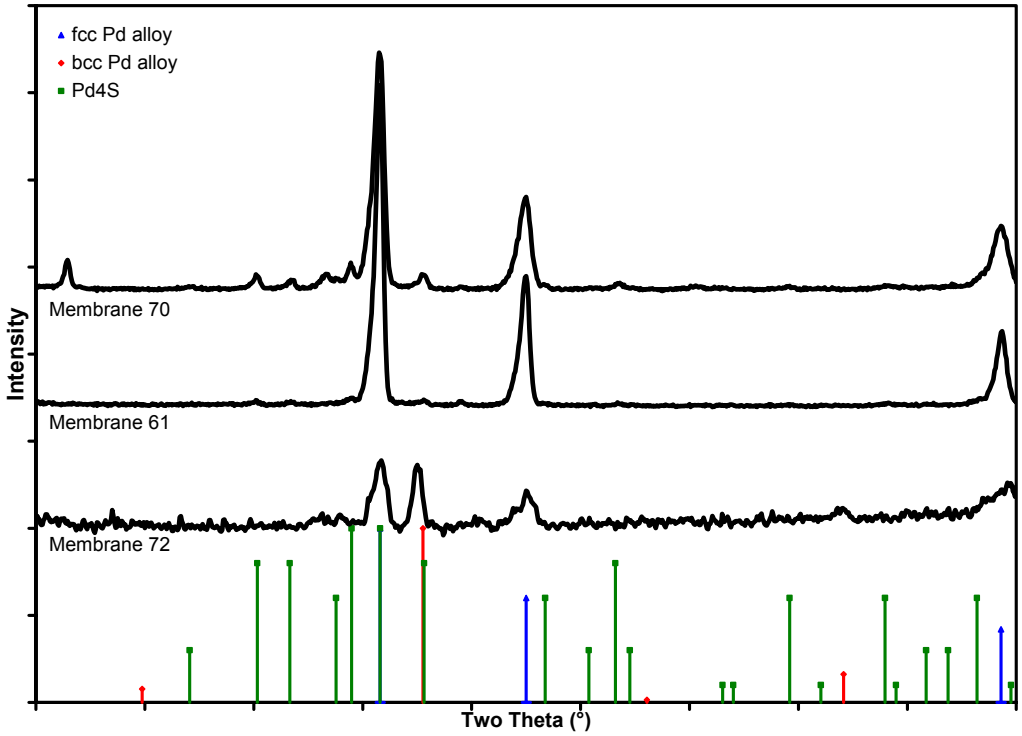

Figure 39: XRD Scans of Membranes 70, 61 and 72

The results of the EDX and XRD analyses are summarized in Table VII. Presented in the table are the Pd concentration in the external portion of the catalyst layer as measured by EDX, whether sulfur was detectable in the external portion of the catalyst layer by EDX, the crystalline phases detected within the catalyst coating, the Pd content of the fcc phase of the coating and the results of a mass balance comparing the amount of non-Pd alloy material originally plated on the membrane to that measured by XRD.

Table VII: Physical Characteristics of Selected Membranes

Membrane ID	Catalyst Pd Concentration by EDX (%)	S detected by EDX?	XRD Phases	fcc Alloy Pd Concentration by XRD (%)	Unaccounted Alloy Component (%)
58	87	yes	fcc alloy & Pd_4S	82	52
70	77	no	fcc alloy & Pd_4S	78	53
61	77	no	fcc alloy & v. wk. Pd_4S	78	27
72	71	no	fcc alloy & bcc alloy	75	3

The poor activity of Membrane 72 (and other membranes not shown here) was strongly correlated with the presence of the bcc Pd alloy phase in the catalyst coating. Membranes with fcc Pd alloy coatings exhibited permeabilities several times that of pure Pd in pure H_2 streams.

The source of high sulfur tolerance in Membranes 58 and 70, relative to that of Membrane 61 is more difficult to ascertain. The external coating of all three membranes contained traces of palladium sulfide, with the presence of Pd_4S most evident in Membrane 58. The Pd content of the fcc alloy was identical in Membranes 70 and 61, so it is unlikely that the sulfur tolerance arose from differences in the primary crystalline phase of the catalyst coatings.

There is an amount of metallic alloy component that is not accounted for in the XRD analysis or EDX analysis of each membrane. The discrepancy between the amount loaded and the amount detected is most significant for the two membranes that are most sulfur tolerant. Since the analysis depth of both EDX and XRD is less than the thickness of the analyzed coatings, it is possible that there is a variation in catalyst composition in the vicinity of the substrate-coating interface that affects membrane performance. Attempts to quantify compositional gradients near the substrate-coating interface via EDX and AES were not successful.

5. WATER GAS SHIFT MEMBRANE REACTOR DEVELOPMENT

In order to demonstrate an integrated water gas shift membrane reactor with larger H_2 production rate, a prototype 1 L H_2/h reactor was designed and constructed. This reactor was similar in design to the membrane permeation test system used in Section 4, but was wider and longer in order to accommodate longer membranes and water gas shift catalyst. The system was initially loaded with a blank (impermeable) membrane tube to reconfirm water gas shift reaction activity and evaluate means by which to minimize direct contact between the catalyst and membrane surface.

The geometry of the WGS membrane reactor hardware dictated that the reaction be conducted at lower space velocities than demonstrated in Section 3. The water gas shift performance of MCP-3 sulfur-tolerant WGS catalyst was confirmed in the new water gas shift membrane reactor equipped with a blank membrane tube. Following a modified activation procedure, the catalyst was exposed to a syngas stream containing 60.0% CO, 23.7% H_2, 10.3% CO_2, 5.0% N_2, and 0.3% H_2S at 425°C, 225 psig and a H_2O/CO ratios ranging from 0.8 to 3.0 (Figure 40). As expected, equilibrium CO conversions were observed at all conditions. No ill-effects from operating at a H_2O/CO ratio of 0.8 were observed.

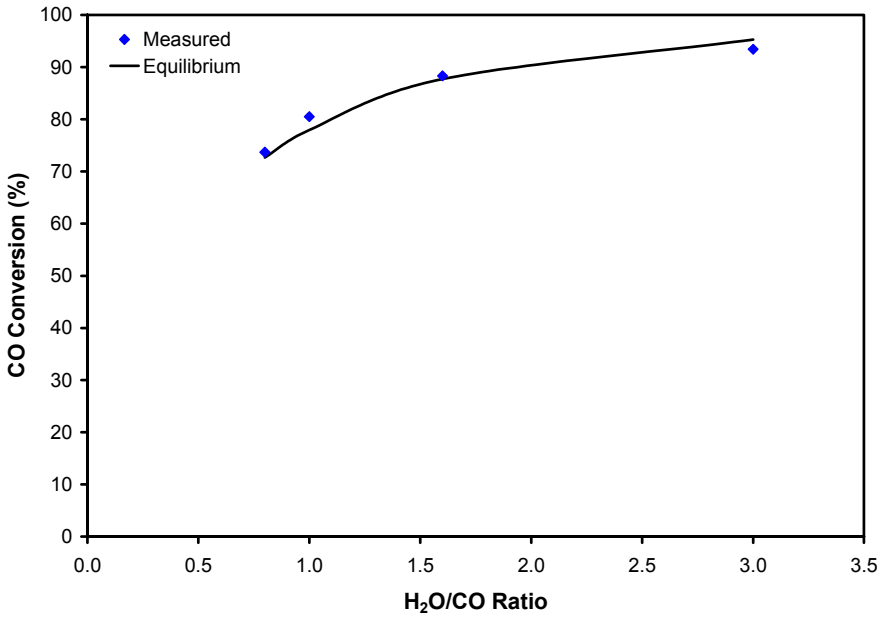

Figure 40: CO Conversion in Water Gas Shift Reactor at 1400 h^{-1} GHSV
(23.8% H_2, 60.6% CO, 10.3% CO_2, 5.0% N_2, 3000 ppm H_2S; Temp.=425°C; Press.=225 psig; GHSV=1400 h^{-1})

An inorganic fiber layer was wrapped around the tubular membrane in this test in order to prevent direct contact of the catalyst with the membrane surface. Discoloration of the membrane in one area which was left unprotected was observed upon disassembly of the reactor following WGS testing. This confirmed that contact of the catalyst and membrane under reaction conditions can affect the membrane surface composition. It was uncertain whether this contact would have adverse effects on the performance of the membrane, but in all future WGS membrane builds, a thin porous separator was used to prevent catalyst-membrane contact.

The blank membrane was then replaced with a H_2-permeable tubular membrane (74% Pd alloy, 6 micron coating). Fresh MCP-3 catalyst was loaded into the membrane reactor and the reactor was mounted in the test stand. Following a baseline measurement with a H_2/He mixture at 150 psig, the reactor was fed with gas streams containing 2000 H_2S and 33% H_2O to confirm membrane performance. Following an additional purging with H_2/He, simulated coal gas containing 16% H_2, 37% CO, 37% H_2O, 6% CO_2, 3% N_2 and 2000 ppm H_2S (H_2O/CO ratio of 1.0) was fed to the membrane reactor at 225 psig (Figure 41).

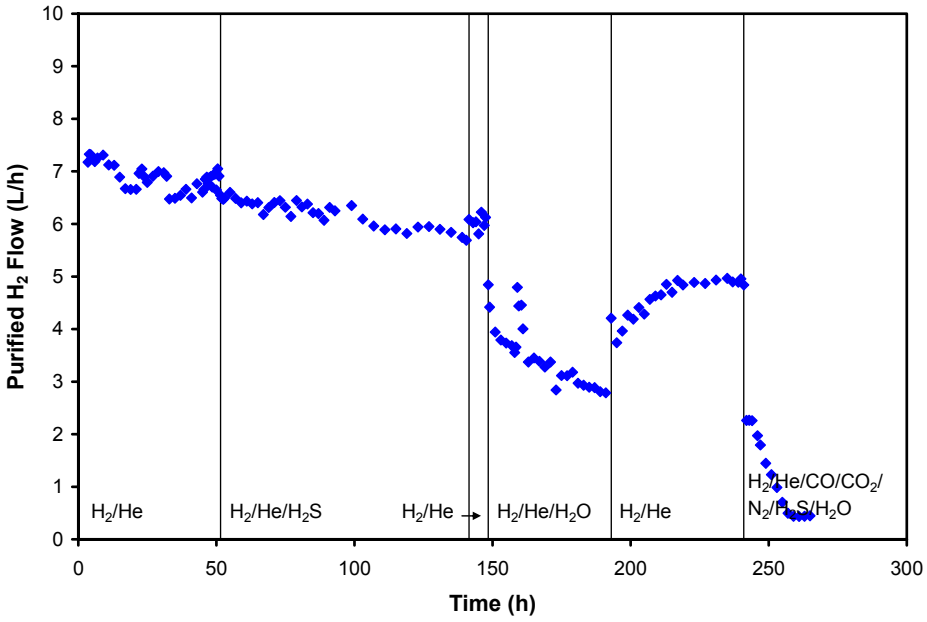

Figure 41: H_2 Production from Water Gas Shift Membrane Reactor

Although initial hydrogen production was greater than usual (permeability of 8.8 x 10^{-8} mol/m/s/$Pa^{0.5}$), a steady decrease in hydrogen production was observed in the presence of H_2 and H_2S. An additional decrease in hydrogen flux (partially reversible, partially irreversible) was observed when exposed to 33% water. Upon exposure to simulated coal gas, the H_2 production rate decreased to 0.5 L/h. The gradual decrease in permeation seen in the presence of H_2, H_2S and H_2O was atypical for a membrane prepared with multiple coating layers. After additional analysis, it was concluded that the reactor was operated at too low a H_2O/CO ratio, and that high CO concentrations likely led to rapid deterioration of permeability upon exposure to the simulated coal gas. Prior to exposure to the simulated coal gas, 73% of the hydrogen fed to the membrane reactor was recovered as purified H_2.

A second membrane (72% Pd alloy, 7 micron coating) was loaded into the membrane reactor with fresh MCP-3 catalyst. The membrane was exposed to streams containing 95% H_2 + 5% He, 90.1% H_2 + 4.2% CO + 4.7% He, and 61.8% H_2 + 2.9% CO + 3.2% He + 31.4% H_2O at pressures of 150 and 225 psig (Figure 42). The CO and H_2O concentrations in this test correspond to those expected in a WGS membrane reactor operating on coal-derived syngas containing 59.7% CO, 25% H_2, 10% CO_2, 5% N_2, 0.3% H_2S (dry basis) at 415°C, 225 psig and a H_2O/CO ratio of 2.0. The H_2 permeability of the membrane remained at 4 x 10^{-8} mol/m/s/$Pa^{0.5}$ throughout the 78 h test. An average purified H_2 flow of 3.3 L/h was demonstrated from the membrane reactor, which was 1.5 inches in length. The gas chromatograph impurity detection

limit for CO, CO_2 and He were each approximately 100 ppm_v, so the purity of the permeated hydrogen was estimated to be at least 99.97%.

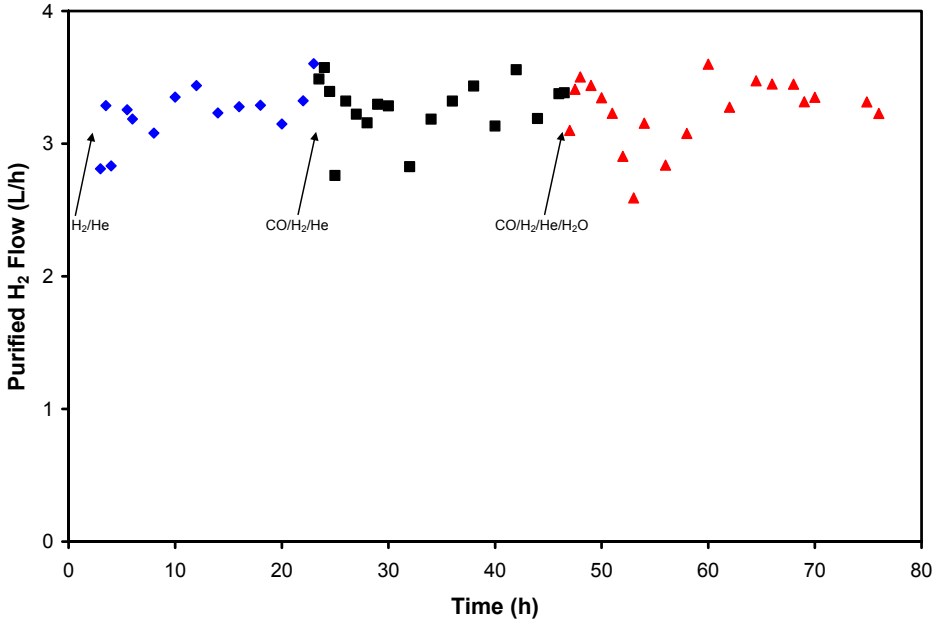

Figure 42: Effect of Simulated Coal Gas on Purified H_2 Flow

6. COST ANALYSIS

Analyses of the costs of producing the H_2-permeable membrane and the contaminant-tolerant water gas shift catalyst were conducted. The analyses assumed large volume production of these components in which the costs of some raw materials were driven down to near bulk commodity prices.

The membrane characteristics used as a basis for the membrane cost estimate are presented in Table VIII. Tantalum and palladium historical prices are summarized in Figure 43. The Ta price used in the cost estimate was the spot price plus 20% ($57.60/lb), to account for the cost of forming into desired geometries, while the Pd price used was the spot price plus 25% ($356/oz) to account for the cost of Pd precursor preparation.

Table VIII: Membrane Characteristics

Ta substrate thickness	255 micron
External catalyst coating Pd content	68 %
External catalyst coating thickness	2.5 micron
Internal catalyst coating Pd content	100 %
Internal catalyst coating thickness	0.5 micron

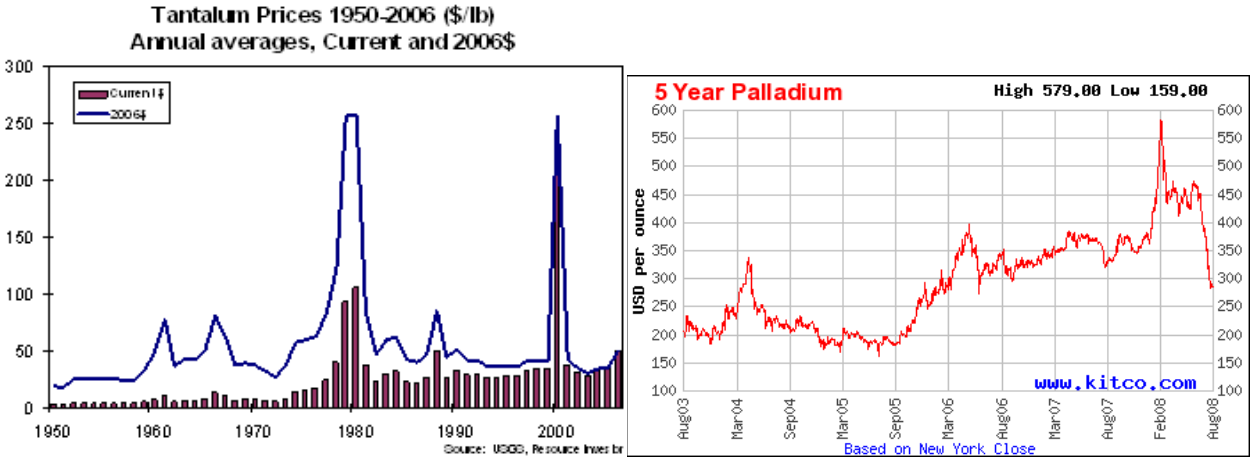

Figure 43: Spot Market Prices of Tantalum[5] and Palladium[6]

Large scale production of the H_2-permeable membrane summarized in Table VIII requires 395 g of tantalum, 2.1 g of palladium, and 275 g of other metal components and electroless plating reactants per square foot of membrane area. The total membrane raw materials cost was estimated to be $88/sq ft. The cost breakdown of the raw materials required for membrane production is summarized in Figure 44. Ta and Pd are the dominant components of the raw materials cost.

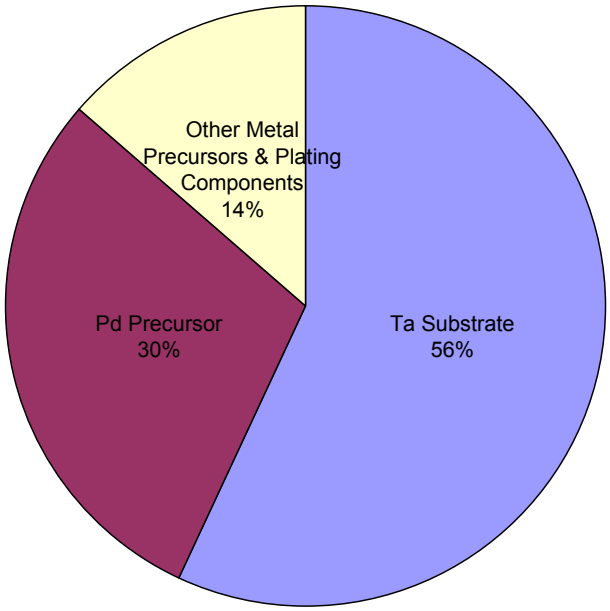

Figure 44: H_2 Permeable Membrane Raw Materials Cost Breakdown

There do not appear to be any significant impediments to scale-up of the membrane electroless plating process. A block diagram that summarizes the processing steps required to produce the coated membranes starting from drawn tantalum tube or sheet is provided in Figure 45. The production process is very similar to that used for industrial electroplating, consisting of a series of batch processes generally comprising cleaning, activation, plating and finishing. Multiple electroless plating steps are required in order to build up the desired layers of catalyst on the membrane surface.

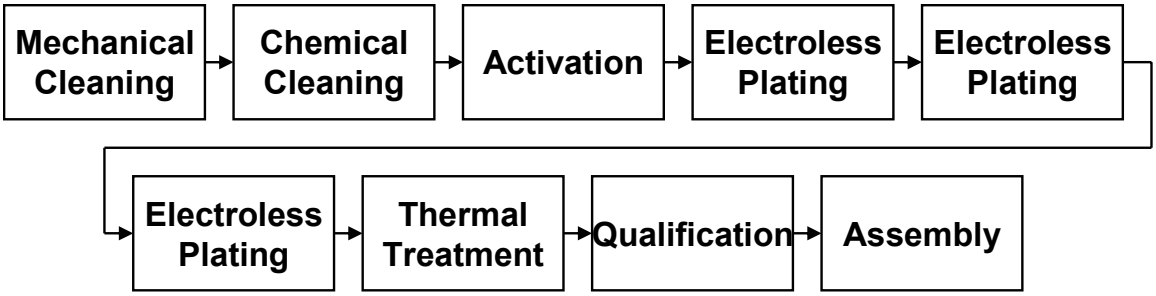

Figure 45: Membrane Production Process

The cost of the contaminant-tolerant water gas shift catalyst is small relative to that of the H_2 permeable membrane. At a flux of 32 scf H_2/h/sqft membrane and a space velocity of 3000 h^{-1}, only 373 g of water gas shift catalyst is required per square foot of membrane area. At an estimated catalyst raw materials cost of $18/kg (Figure 46), the catalyst cost per square foot of

membrane is $6.65. The majority of the cost is attributable to the molybdenum precursor used in the development program, which was priced at $103/kg.

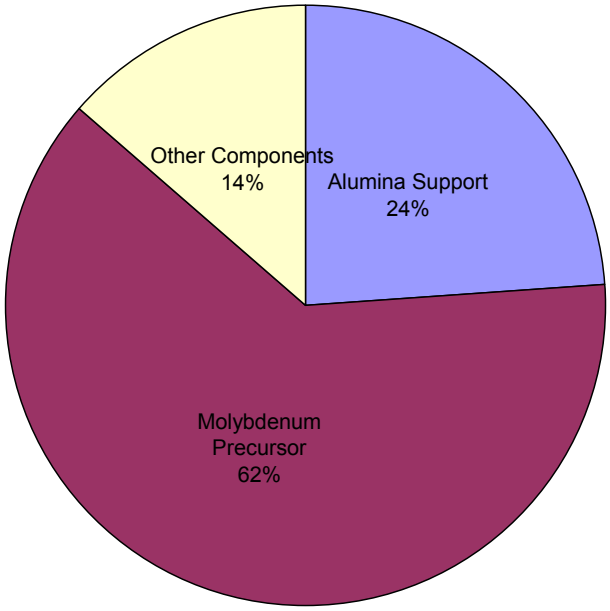

Figure 46: Water Gas Shift Catalyst Raw Materials Cost Breakdown

No significant impediments to manufacturing of the catalyst exist. Conventional catalyst impregnation techniques and equipment can be used to prepare the contaminant-tolerant water gas shift catalyst.

7. CONCLUSIONS

A water gas shift catalyst and hydrogen-permeable membrane that were tolerant of contaminants commonly found in coal-derived syngas were developed in this program. Both materials met most of the Department of Energy 2015 Hydrogen from Coal RD&D water gas shift catalyst and membrane development targets.

The water gas shift catalyst outperformed commercial high temperature shift and sour gas shift catalysts under the conditions experimentally examined. The high activity was attributed to the high catalyst surface area and use of catalyst dopants not commonly used in commercial water gas shift catalysts. Equilibrium carbon monoxide conversions were achieved with high steam content syngas streams (H_2O/CO=4, 500°C, 400 psig, 12,000 h^{-1} space velocity) and with drier syngas streams (H_2O/CO=0.8, 425°C, 225 psig, 1,400 h^{-1} space velocity). The most active and stable catalyst was operated for over 110 hours in the presence of 3000 ppm H_2S and 350 ppm HCl without irreversible degradation of catalytic activity.

A summary of the characteristics of the water gas shift catalyst relative to DOE targets is presented in Table IX. The developed catalyst meets or exceeds the 2015 development targets for approach to equilibrium, H_2O/CO ratio, sulfur tolerance and chloride tolerance. Further testing is required to evaluate catalyst ability to meet temperature, pressure, COS conversion and durability targets. While the catalyst cost exceeds the target, it does not require the use of any particularly expensive precursors (i.e. no precious metals). Reformulation with an alternative molybdenum precursor may reduce the projected cost.

Performance Criteria	Current Status	Targets		This Work
		2010	2015	
Catalyst Form	Pellets	Advanced configurations – TBD		Pellets
Active Metal	Cu/Zn or Fe/Cr or Co/Mo	Advanced configurations – TBD		Mo
Feed Temperature (°C)	200-300	>250	>400	>250
Feed Pressure (psia)	450-1150	>450	>750	415
Approach to Equilibrium (°C)	8-10	<6	<4	<4
Min. H_2O/CO Ratio	2.6	<2.6	<2	<2
Sulfur Tolerance (ppm_v)	varies	>20	>100	3000
COS Conversion	varies	Partial	Total	-
Chloride Tolerance (ppm_v)	varies	>3	>100	350
Durability (y)	3-7	>7	>10	-
Catalyst Cost ($/lb)	~5	<5	<5	~8

Table IX: DOE Catalyst Development Targets and Demonstrated Capabilities

The hydrogen permeable membrane was composed of a layered structure in which a highly permeable dense tantalum layer was sandwiched between coatings of Pd alloy that exhibited high catalytic activities and tolerance to sulfur. Membrane permeability was approximately six times that of Pd, but hydrogen flux was lower than many Pd membranes due to membrane thickness requirements. Some hydrogen embrittlement occurred in the membrane at low temperature and high pressure, but was managed by controlling the operating environment of the membrane. Hydrogen purity in excess of 99.97% was routinely demonstrated.

Catalyst composition was found to play a critical role in maintaining hydrogen permeability in the presence of hydrogen sulfide, while catalyst coating integrity and annealing temperature were

the key determinants of membrane stability in the presence of steam. Good membrane stability was demonstrated in the presence of 2000 ppm H_2S, maintaining a hydrogen permeability of $7x10^{-8}$ mol/m/s/$Pa^{0.5}$ at 425°C. Although a long-term durability test of the best-performing membrane was not conducted, routine screening of membrane formulations often lasted over 150 hours.

Good adhesion between the membrane catalyst coating and substrate was observed following hydrogen permeation tests. Membrane characterization revealed that the presence of a face centered cubic lattice structure in the Pd alloy was necessary, but not sufficient, for sulfur tolerance.

A summary of the characteristics of the hydrogen-permeable membrane relative to DOE targets is presented in Table X. The membrane meets or exceeds 2015 targets for sulfur tolerance, cost and hydrogen purity. Additional testing is required to evaluate water gas shift activity and durability, while additional materials development is required to achieve hydrogen flux and pressure targets.

Performance Criteria	Current Status			Targets			This Work
	Microporous	Cermet	Dense Ceramic	2007	2010	2015	
Flux (scfh/ft^2)	20-100	~220	2	100	200	300	32
Temperature (°C)	300-600	300-400	900	400-700	300-600	250-500	350-500
S Tolerance (ppm_v)	Yes	~20	-	-	20	>100	3000
Cost ($/$ft^2$)	150-200	<200	-	150	100	<100	~88
WGS Activity	No	-	-	Yes	Yes	Yes	-
ΔP Capability (psig)	100	1000	-	100	400	800	400
CO Tolerance	Yes	Yes	-	Yes	Yes	Yes	Yes
H_2 Purity (%)	90-98	>99.999	-	95	99.5	99.99	>99.97
Durability (y)	-	0.9	-	1	3	5	-

Table X: DOE Membrane Development Targets and Demonstrated Capabilities

Because the water gas shift catalyst and hydrogen-permeable membrane can be operated in the same environment at the same temperature and pressure, they can be easily integrated into a catalytic membrane reactor for one-step production of purified hydrogen. Because the carbon monoxide tolerance of the membrane was limited to less than 5 vol%, a staged membrane reactor in which much of the shift reaction occurs upstream of the membrane element must be employed to purify coal-derived syngas streams.

Additional studies are required to answer some of the unresolved questions regarding the developed technology and improve performance to meet DOE goals. In order to improve hydrogen flux, the thickness of the membrane substrate must be reduced. To avoid mechanical failure of the thinner membrane, less embrittling metal alloys must be developed and employed as the substrate. While membrane sulfur tolerance was demonstrated, as the membrane substrate becomes thinner, the role that the catalytic coating plays in the permeation process becomes more significant, and a more thorough understanding of why particular alloy catalysts perform better than others would be beneficial.

This program demonstrated the benefits of using a multifunctional membrane for purifying contaminant-laden syngas. By selecting one material with high hydrogen permeability and

another material with high reactivity and tolerance to impurities, the performance of the composite membrane can be tuned to achieve maximum performance.

8. REFERENCES

[1] available at http://fossil.energy.gov/programs/fuels/publications/programplans/2007_Hydrogen_Program_Plan.pdf
[2] Steward, LLNL Report, UCRL-53441 (1983)
[3] Rothenberger *et al.*, *J. Membr. Sci.*, 218, 19 (2003)
[4] Makrides *et al.*, Contract DA-49-189-AMC-136(d) (1965)
[5] Tantalum Prices available at http://www.resourceinvestor.com/pebble.asp?relid=28252
[6] Palladium Prices available at http://www.kitco.com/charts/livepalladium.html